Estimating Radiative Forcing Efficiency of Dust Aerosol Based on Direct Satellite Observations: Case Studies over the Sahara Desert and Taklimakan Desert

Lin Tian[1,2,3], Lin Chen[3], Peng Zhang[3], Lei Bi[4]

[1] Nanjing University of Information Science & Technology, Nanjing, China.

[2] Chinese Academy of Meteorological Sciences, Beijing, China.

[3] National Satellite Meteorological Center, China Meteorological Administration, Beijing, China.

[4] Department of Atmospheric Sciences, School of Earth Sciences, Zhejiang University, Hangzhou, China.

Correspondence to: Peng Zhang (zhangp@cma.gov.cn) & Lin Chen (chenlin@cma.gov.cn)

Abstract. The direct radiative forcing efficiency of the dust aerosol ($DRFE_{dust}$) is an important indicator to measure the climate effect of the dust. The $DRFE_{dust}$ is determined by the microphysical properties of the dust, which vary with the dust source regions. However, there are only sparse in-situ measurements of them, such as the distribution of the dust aerosol particle size and the complex refractive index in the main dust source regions. Furthermore, recent studies have shown that the non-spherical effect of the dust particle is not negligible. The $DRFE_{dust}$ is often evaluated by estimating given microphysical properties of the dust aerosols in the radiative transfer model (RTM). However, considerable uncertainties exist due to the complex and variable dust properties, including the complex refractive index and the shape of the dust. The $DRFE_{dust}$ over the Taklimakan Desert and the Sahara Desert is derived from the satellite observations in this paper. The advantage of the proposed satellite-based method is that there is no need to consider the microphysical properties of the dust aerosols in estimating the $DRFE_{dust}$. For comparison, the observed $DRFE_{dust}$ is compared with that simulated by the RTM. The differences in the dust microphysical properties in these two regions and their impacts on $DRFE_{dust}$ are analyzed.

The $DRFE_{dust}$ derived from the satellite observation is -39.6 ± 10.0 $Wm^{-2}\tau^{-1}$ in March 2019 over Tamanrasset and -48.6 ± 13.7 $Wm^{-2}\tau^{-1}$ in April 2019 over Kashi. According to the analyses of their microphysical properties and optical properties, the dust aerosols from the Taklimakan Desert (Kashi) scatter strongly. The RTM simulated results (-41.5 to -47.4 $Wm^{-2}\tau^{-1}$ in the Taklimakan Desert and -32.2 to -44.3 $Wm^{-2}\tau^{-1}$ in the Sahara Desert) are in good agreement with the results estimated by satellite observations. According to previous studies, the results in this paper are proved to be

reasonable and reliable. The results also show that the microphysical properties of the dust can significantly influence the $DRFE_{dust}$. The satellite-derived results can represent the influence of the dust microphysical properties on the $DRFE_{dust}$, which can also validate the direct radiative effect of the dust aerosol and the $DRFE_{dust}$ derived from numerical model more directly.

1 Introduction

Dust aerosols are considered to be one of the major components of the tropospheric aerosols (Huneeus et al., 2012;Textor et al., 2007). The dust aerosols affect the radiation balance of the earth-atmosphere system by scattering and absorbing solar radiation directly (Miller et al., 2014;Satheesh, 2002). Estimating the direct radiation effect of the dust aerosol (DRE_{dust}) is crucial for estimating climate forcing. The scattering of the dust influences the radiation in the shortwave (SW) spectrum at the top of atmosphere (TOA), which causes stronger SW DRE_{dust} over dust source regions (Slingo et al., 2006). Therefore, the evaluation of SW DRE_{dust} is important for climate modeling.

The variabilities of the mineral dust composition from soils in different source regions cause the differences in dust microphysical properties (e.g., refractive index, size, and particle shapes). The Direct Radiative Forcing Efficiency of the dust aerosol ($DRFE_{dust}$) is defined to quantify the dust radiative effect (Anderson et al., 2005;Satheesh and Ramanathan, 2000). The $DRFE_{dust}$ represents the DRE_{dust} of per unit aerosol optical depth (AOD), which means the efficiency of the dust aerosol that affects the net radiative flux of solar radiation. The $DRFE_{dust}$ is largely determined by the optical properties of the dust aerosols (Shi et al., 2005), which are strictly controlled by the microphysical properties of the particles (Di Biagio et al., 2014b;Di Biagio et al., 2017;Di Biagio et al., 2014a;Zhang et al., 2006). Therefore, the $DRFE_{dust}$ is different concerning the dust aerosols from different source regions (Tanré et al., 2001;Che et al., 2012). Without considering the influence of the aerosol loading on the DRE_{dust}, the $DRFE_{dust}$ has unique advantages in evaluating the differences of dust microphysical properties and their impacts on the DRE_{dust} from different dust source regions (García et al., 2008).

The $DRFE_{dust}$ is often estimated by the General Circulation Model (GCM) and the Radiative Transfer Model (RTM). Many studies have simulated the SW $DRFE_{dust}$ in different regions (Valenzuela et al., 2012;Che et al., 2009;Bi et al., 2014). However, there are sparse in-situ measurements of the dust microphysical properties in the main source regions. The large spatial

variability of aerosols and the lack of an adequate database on their properties make DRE_{dust} and $DRFE_{dust}$ much very difficult to be estimated (Satheesh and Srinivasan, 2006). To date, climate models generally use temporal and spatial constant values to represent the dust microphysical properties (Di Biagio et al., 2017;Di Biagio et al., 2014a;Bi et al., 2020). This may cause uncertainties in calculating the dust radiative effect. Moreover, the shape of the dust particle in the model needs to be assumed. Therefore, there are large uncertainties in estimating the $DRFE_{dust}$ with few measurements of the dust microphysical properties from different source regions (Bi et al., 2020;Colarco et al., 2014;Zhao et al., 2013).

Satellite observations can be used in estimating the $DRFE_{dust}$ because satellites can directly observe the radiation budget of the earth at the TOA (Wielicki et al., 1998;Satheesh and Ramanathan, 2000), and the remote-sensing technique for the AOD has been developed (Remer et al., 2005;Hsu et al., 2004). In the previous study, we developed a satellite-based method to estimate the $DRFE_{dust}$ over land without any assumptions of the microphysical properties of dust aerosols (Tian et al., 2019). In previous researches, performances of the models in simulating the dust radiative effect have been indirectly validated by comparing the observations of the AOD, the single scattering albedo (SSA), the distribution of the particle size, and the extinction profile of the aerosols with the simulated ones (Zhao et al. 2010; Chen et al. 2014). Therefore, the satellite-based method provides a direct way to validate the DRE_{dust} and the $DRFE_{dust}$.

The Sahara Desert and the Taklimakan Desert are the main dust source regions, which influence many areas (Li et al., 2020;Mikami et al., 2006;Mbourou et al., 1997;Huang et al., 2014). Previous studies also estimated the $DRFE_{dust}$ in the Sahara Desert and the Taklimakan Desert (Li et al., 2020;Li et al., 2004;Garc á et al., 2012;Xia and Zong, 2009). Garc á et al. (2012) evaluated the $DRFE_{dust}$ in the Sahara Desert based on the Global Atmospheric ModEl (GAME) and the AERONET retrievals. Li et al. (2004) estimated $DRFE_{dust}$ in the Sahara Desert based on the satellite data and the SBDART model. For the Taklimakan Desert, Li et al. (2020) estimated the instantaneous SW $DRFE_{dust}$ based on the RTM and ground-based measurements of dust properties. Xia and Zong (2009) used both the satellite data and the SBDART model to represent the instantaneous SW $DRFE_{dust}$ at the TOA (Xia and Zong, 2009). The $DRFE_{dust}$ varies in these studies, and the differences may come from the different research conditions and the difference of dust aerosol microphysical properties in the Sahara Desert and the Taklimakan Desert. Thus, the assessment on the SW $DRFE_{dust}$ and dust microphysical properties over

the Sahara Desert and the Taklimakan Desert is meaningful to evaluate regional and global climate changes.

In this paper, the $DRFE_{dust}$ at the TOA in dust storms over the Taklimakan Desert and the Sahara Desert is evaluated based on satellite observations and the RTM, separately. With the comparison of the dust microphysical properties and the $DRFE_{dust}$ at the TOA in these two regions, the differences of the dust microphysical properties are analyzed. Meanwhile, the influences of the dust microphysical properties on the $DRFE_{dust}$ at the TOA are investigated in this paper. The need for accurate information on the dust microphysical properties and dust sources for simulating the $DRFE_{dust}$ is emphasized, and the advantage of the satellite-based method in estimating the $DRFE_{dust}$ is revealed.

2 Methodology and data

In the previous study (Tian et al., 2019), the equi-albedo method has been proposed to estimate the DRE_{dust} and the $DRFE_{dust}$ at the TOA over land based on satellite measurements directly. This method bases on the assumption that the SW radiative fluxes at the TOA of the clear sky (F_{clr}) are equal over the regions with similar land surface albedo (LSA) and solar zenith angle (SZA). Following this method, we estimated the $DRFE_{dust}$ based on the AOD and the SW radiative flux product from the same satellite platform.

Moreover, the $DRFE_{dust}$ in the RTM with dust aerosol microphysical properties is also evaluated. Based on the comparison between the $DRFE_{dust}$ results from the two methods, the differences in the dust microphysical properties over the Taklimakan Desert and the Sahara Desert are analyzed, and the differences in the $DRFE_{dust}$ at the TOA are also discussed. The processing steps are shown in Fig. 1.

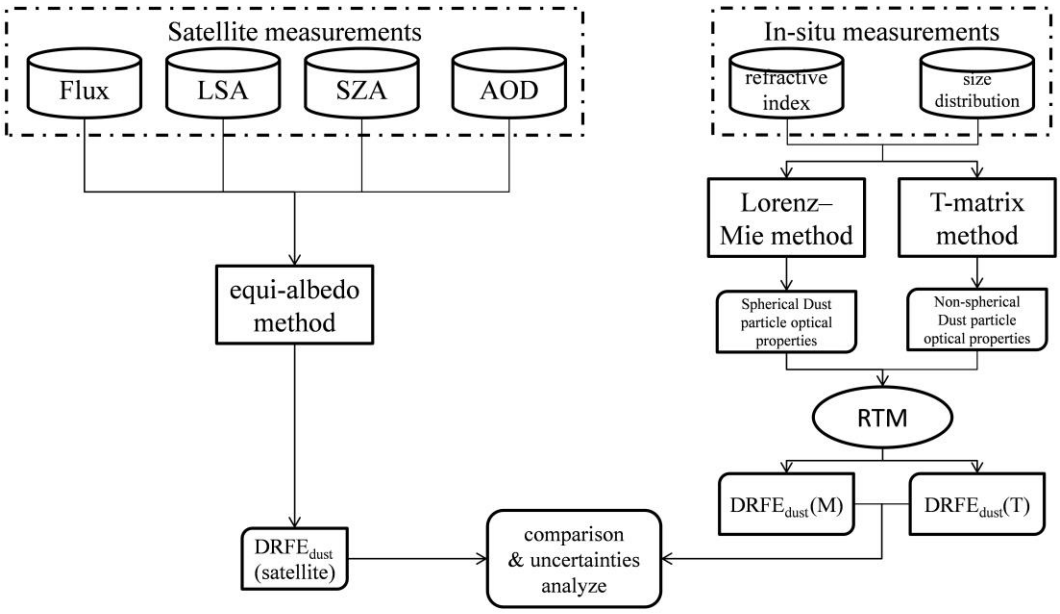

Flux: Radiative Flux observed by CERES;
LSA: Land Surface Albedo;
SZA: Solar zenith Angle;
AOD: Aerosol Optical Depth;
$DRFE_{dust}$(satellite): $DRFE_{dust}$ estimated from satellite measurements
$DRFE_{dust}$(M): $DRFE_{dust}$ simulated from Lorenz–Mie method and RTM;
$DRFE_{dust}$(T): $DRFE_{dust}$ simulated from T-matrix method and RTM;

Figure 1: Processing flow chart of this paper.

2.1 Methodology

2.1.1 The equi-albedo method

Previous studies have shown that F_{clr} is significantly influenced by the LSA and the SZA at the TOA (Di Biagio et al., 2012;Tegen et al., 2010). It is hard to assess the SW DRE_{dust} and the $DRFE_{dust}$ over land derived from satellite observations due to the large dynamic range of the LSA (Satheesh, 2002). In the previous study (Tian et al., 2019), we proposed an equi-albedo method to minimize the influence of the inhomogeneous LSA and SZA and directly derived the DRE_{dust} and the $DRFE_{dust}$ over land from satellite observations based on the assumption that the F_{clr} is equal over the regions with similar LSA and SZA.

DRE_{dust} is defined as the upward radiative flux difference between clear (F_{clr}) and dust loading (F_{dust}) conditions (Garrett and Zhao, 2006;Christopher et al., 2000;Ramanathan et al., 1989).

$$DRE_{dust} = F_{clr} - F_{dust} \quad (1).$$

F_{dust} is the shortwave radiative flux at the TOA under the cloud-free and dust aerosol loading conditions which is obtained directly from the Clouds and the Earth's Radiant Energy System (CERES).

F_{clr} is the shortwave flux over the same region without aerosol. F_{clr} cannot be observed directly, and the estimating of F_{clr} must be on the basis of some realistic assumptions.

The equi-albedo method bases on the assumption that the upward SW radiative flux at the TOA of the clear sky (F_{clr}) are equal over the regions with similar land surface albedo (LSA) and solar zenith angle (SZA). In the equi-albedo method we set the cloud-free pixels with AOD smaller than 0.1 as the clear-sky pixels (Tian et al., 2019). Therefore, it can be considered to be in the same condition when the difference between LSA is less than 0.01, and the difference between SZA is less than 0.2 º. This keeps good consistency of F_{clr} between clear and dust storm area, and ensures that enough pixels could match the condition (Tian et al., 2019). Based on the assumption, the F_{clr} is estimated, and then DRE_{dust} can be derived following Eq. (1). According to the definition of $DRFE_{dust}$, it represents the net flux of solar radiation perturbed by per unit dust AOD. Therefore, $DRFE_{dust}$ can be expressed as:

$$\mathrm{DRFE_{dust}} = \mathrm{DRE}_{dust}/\tau_{\mathrm{dust}} \quad (2)$$

where τ_{dust} is the AOD of dust aerosols, and τ_{dust} comes from the MODIS aerosol product. Thus, $DRFE_{dust}$ is estimated based on the AOD and the SW radiative flux product from the same satellite platform.

In the previous study (Tian et al., 2019), we have estimated the DRE_{dust} and the $DRFE_{dust}$ of two dust storms in the Taklimakan Desert. The results were compared with the DRE_{dust} and the $DRFE_{dust}$ simulated by the RTM. The results indicated that the method is effective in estimating the SW $DRFE_{dust}$ over land. The microphysical properties of dust aerosols significantly influence on the DRE_{dust} and the $DRFE_{dust}$ (Che et al., 2012;Li et al., 2018). The different microphysical properties of dust aerosols in various dust source regions cause uncertainties in estimating the SW DRE_{dust} and $DRFE_{dust}$. Thus, the equi-albedo method is used to estimate the SW $DRFE_{dust}$ directly using satellite observations in this study. Based on the comparison of the $DRFE_{dust}$ in the Taklimakan Desert and the Sahara Desert, the differences of dust microphysical properties in these two regions are analyzed and the influences of the dust microphysical properties on estimating the $DRFE_{dust}$ are tested.

2.1.2 Calculating method of dust optical properties

Dust aerosols are often assumed as spherical particles in the GCM and the RTM (Wang et al., 2013;Gao and Anderson, 2001). The Lorenz-Mie theory is used to calculate the optical properties of the dust particles (Gouesbet and Gréhan, 2011). However, observations and researches have shown that

most dust aerosols are non-spherical in nature (Nakajima et al., 1989;Okada et al., 2001). Previous researches also suggested that assuming particles as spherical or non-spherical has significant impacts on calculating the dust optical properties (Kalashnikova and Sokolik, 2004;Borghese et al., 2007). Therefore, the optical properties of dust aerosols are calculated using both the spherical and the ellipsoidal methods for comparison to analyze the uncertainties caused by the assumption of dust shapes in estimating the $DRFE_{dust}$ in this study.

To make it more accurate, the light scattering properties of spherical particles are generally calculated based on the Mie and Lorenz theory (Mishchenko and Travis, 2008). Among several methods for computing optical properties of non-spherical particles, the T-matrix method has been extensively developed to many versions for various applications (Chylek et al., 1977;Mishchenko et al., 1996). These versions of the available T-matrix codes are accessed from the National Aeronautics and Space Administration (NASA) Goddard Institute for Space Studies (GISS) group. The T-matrix codes are accessed from the National Aeronautics and Space Administration (NASA) Goddard Institute for Space Studies (GISS) group (https://www.giss.nasa.gov/staff/mmishchenko/t_matrix.html). The codes are directly applicable to spheroids and finite circular cylinders, and spheroids are formed by rotating an ellipse about its minor (oblate spheroid) or major (prolate spheroid) axis (Mishchenko and Travis, 1998). The shape and size of a spheroid can be conveniently specified by the aspect ratio. The aspect ratio is greater than 1 for oblate spheroids, smaller than 1 for prolate spheroids, and equal to 1 for spheres. Therefore, Mie scattering method can be regarded as a special case of the T-matrix method. In this study in order to calculate the dust aerosol optical properties, the dust particles are assumed to be a sphere (aspect ratio equals to 1) and an ellipsoid (aspect ratio equals to 0.8). Furthermore, the differences of aerosol optical properties between different shape assumptions are discussed.

2.1.3 RTM

Santa Barbara Disort DISORT Atmospheric Radiative Transfer (SBDART) is an RTM that calculates the plane-parallel radiative transfer of the earth-atmosphere system (Ricchiazzi et al., 1998a). The broadband radiative flux at the TOA and the surface in clear-sky and dusty conditions can be obtained. It is conducive to analyzing the radiative transfer theory in satellite remote sensing and atmospheric energy budget studies. Furthermore, the model can flexibly set up aerosol properties, which is well suited to calculate the radiative effect of different types of aerosols. The SBDART model

has been widely used in estimating the $DRFE_{dust}$ due to its design (Chen et al., 2011;Li et al., 2020;Iftikhar et al., 2018).

In this paper, the dust aerosol optical properties (the SSA and the ASYmmetry parameter, abbreviated as ASY) are calculated using spherical and non-spherical methods. The Aerosol Robotic Network (AERONET) retrieves the physical properties of aerosols including volume size distribution and the complex refractive index, and optical properties including the SSA and the ASY (Dubovik and King, 2000;Dubovik et al., 2006). The LSA from Moderate Resolution Imaging Spectroradiometer (MODIS) surface albedo product, and the default atmospheric profile of SBDART (MID-LATITUDE WINTER) are used as the input parameters for the SBDART model in simulating the $DRFE_{dust}$. In SBDART model, users can define the aerosol spectral dependence by few wavelengths points, and the aerosol optical properties are extrapolated to other wavelengths by a power law (Ricchiazzi et al., 1998b). Therefore, aerosol properties measured at four wavelengths are extrapolated so that flux calculations can be made in any desired wavelength across the shortwave spectrum (McComiskey et al., 2021). Therefore, the DRE_{dust} changing with the AOD due to both dust aerosol microphysical properties (including the complex refractive index and the distribution of the size) and optical properties (including the SSA and the ASY) are simulated by the SBDART model. The impacts of the microphysical properties and the optical properties of the dust aerosol on the $DRFE_{dust}$ at the TOA are analyzed in this study.

2.2 Data

This paper aims to analyze the differences in dust microphysical properties and the $DRFE_{dust}$ at the TOA over the Taklimakan Desert and the Sahara Desert to confirm the influences of dust aerosol microphysical properties on simulating the $DRFE_{dust}$. Also, the advantages of the satellite-based method in estimating the $DRFE_{dust}$ at the TOA are analyzed. Therefore, the $DRFE_{dust}$ over the Taklimakan Desert and the Sahara Desert is estimated by using both satellite observations and dust microphysical properties.

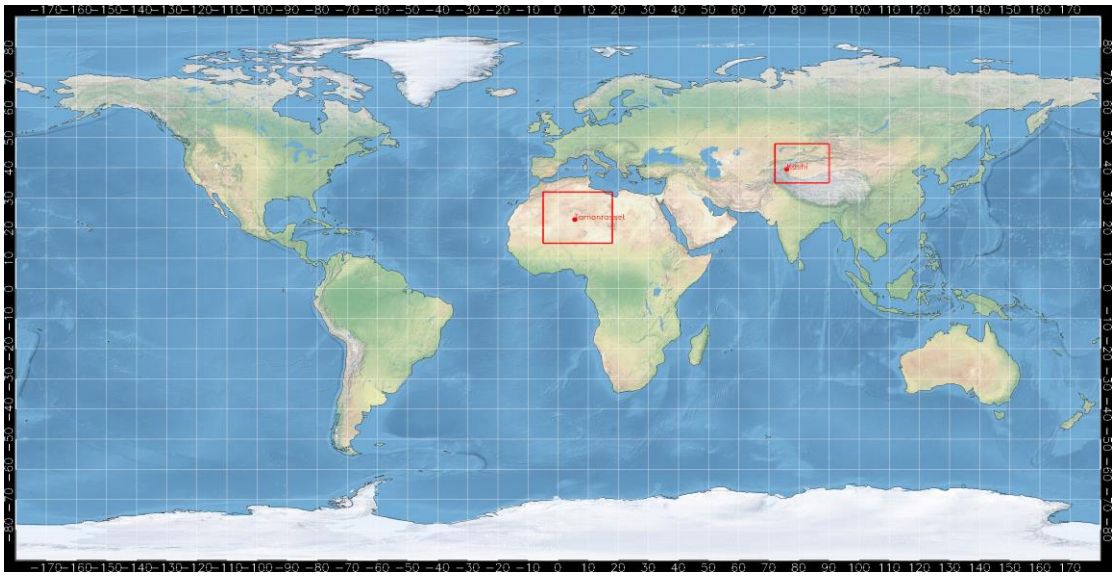

Figure 2: The research regions and dust storms viewed by MODIS AQUA on 11 March and 9 April 2019.

Fig. 2 shows the research regions (the red square areas) and the locations of in-situ sites (Tamanrasset site and Kashi site, the red dots in the map and satellite images). Tamanrasset (22.79˚N, 5.53˚E, 1377 m above the mean sea level) locates in southern Algeria, which is free from the influence of industrial activities. Thus, the aerosols measured in Tamanrasset can represent the pure dust aerosols from the Sahara Desert (Guirado-Fuentes et al., 2014). Kashi (39.5˚N, 75.9˚E, 1320 m above the mean sea level) locates in the vicinity of the Taklimakan Desert. Kashi represents a place affected by dust aerosols transported from the Taklimakan Desert (Li et al., 2020). Thus, dust aerosols observed in Tamanrasset and Kashi sites are typical samples of the dust aerosols from these two deserts. Moreover, Tamanrasset and Kashi sites are similar in land surface type, altitude, and climate. As the LSA and the SZA have a great impact on the SW radiative effect, the regions with similar LSA and SZA are chosen to avoid the influence of different LSA and SZA on evaluating the differences of dust microphysical properties and dust radiative effect from different dust source regions.

Several dust storms occurred on March 9, 11 and 14, 2019 in the Sahara Desert. In the Taklimakan Desert, dust storms occurred on April 9, 23 and 25, 2019. Figure 3 shows the LSA and the SZA observed by the AQUA satellite over the Sahara Desert (Figs. 3(a1)–(a3) and Figs. 3(b1)–(b3)) and Taklimakan Desert (Figs. 3(c1)–(c3) and Figs. 3(d1)–(d3)) during dust storm episodes. In Fig. 3, the LSA and the SZA are similar in Tamanrasset and Kashi when the satellite passes through. The data around Tamanrasset and Kashi in March and April are suitable for analyzing the differences of dust microphysical properties and their influences on the $DRFE_{dust}$.

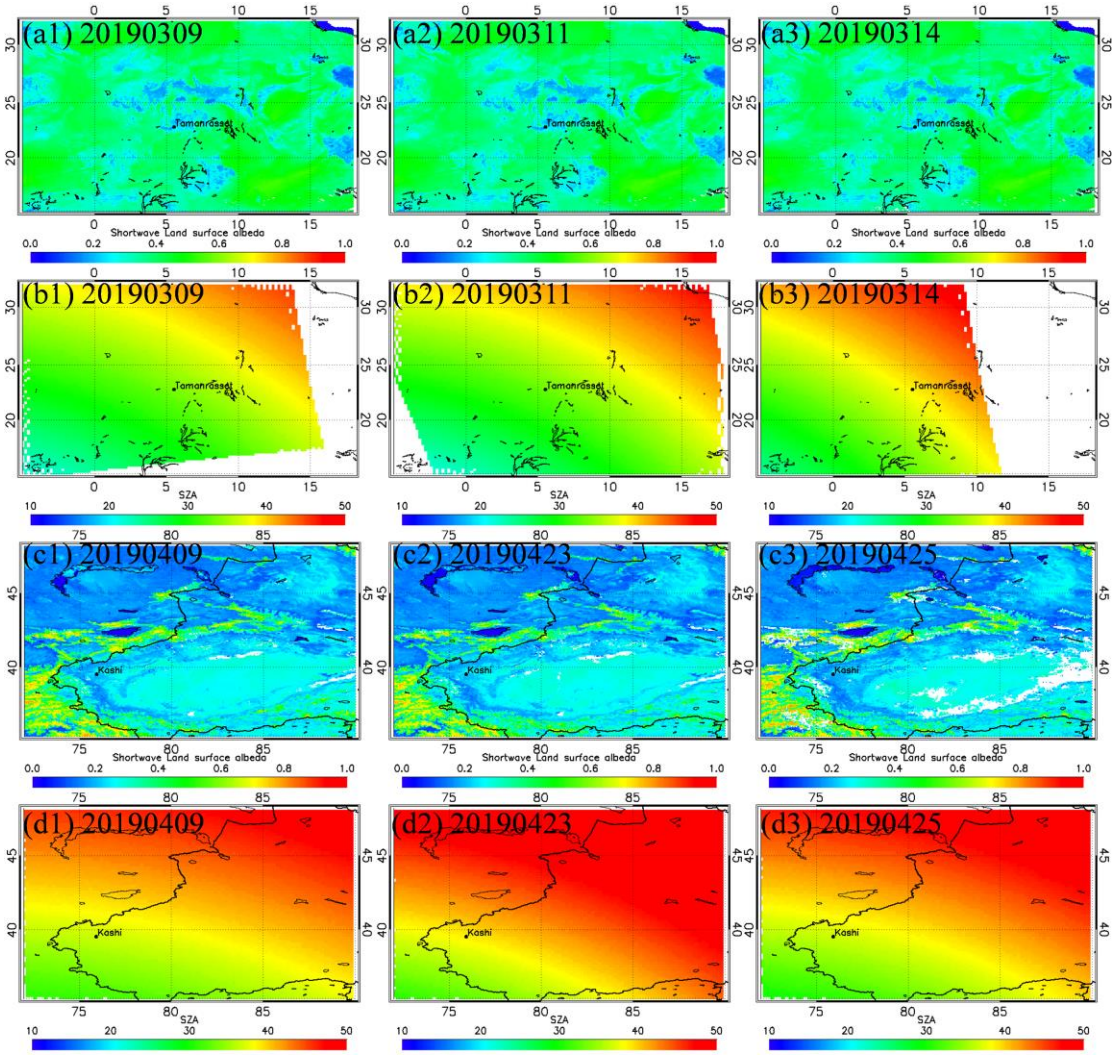

Figure 3: SW LSA and SZA over the Sahara Desert and the Taklimakan Desert derived from AQUA/MODIS.

Figs. 4(a1)–(a3) and Figs. 4(c1)-(c3) present the true color images over the Sahara Desert and the Taklimakan Desert, respectively. Figs. 4(b1)–(b3) and Figs. 4(d1)–(d3) respectively present the cloud detections over the Sahara Desert and the Taklimakan Desert from AQUA/MODIS observations. The satellite crossed over the Sahara Desert on March 9 (UTC 13:05), 11(UTC 12:55) and 14 (UTC 13:20), 2019, and crossed over the Taklimakan Desert on April 9 (07:30), 23 (07:40) and 25 (07:30), 2019. The true color images and cloud detections clearly show that, the Tamanrasset site and Kashi site were not covered by clouds during these dust storms. The satellite-observed and dust microphysical property data of the dust storms in March and April 2019 in Tamanrasset and Kashi are collected to analyze the dust microphysical properties and estimate the $DRFE_{dust}$ in the Sahara Desert and the Taklimakan Desert. Both the satellite data and synergy dust microphysical properties data are collected around Tamanrasset

and Kashi sites for analyzing the differences in dust microphysical properties and estimating the $DRFE_{dust}$.

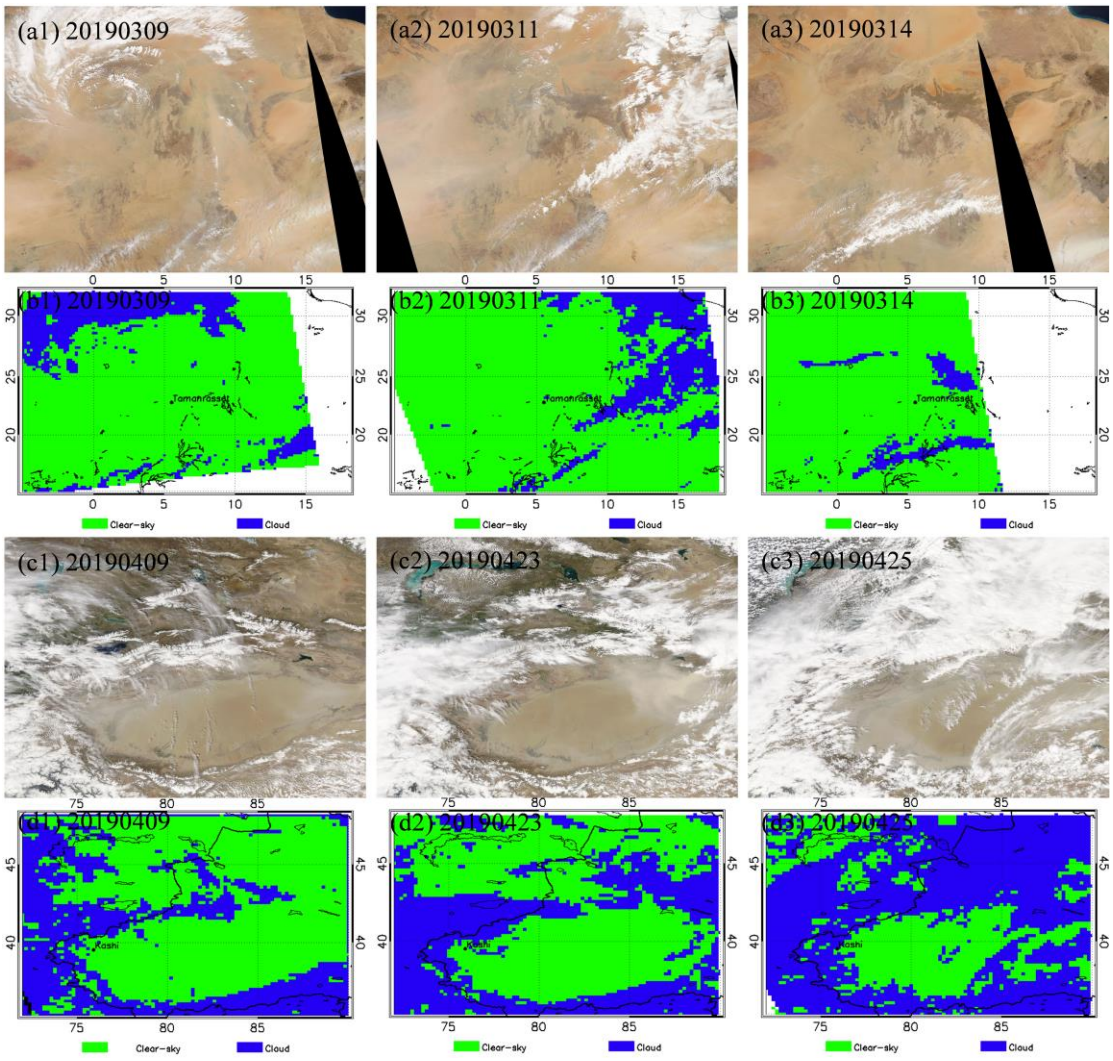

Figure 4: True color images and cloud detections from AQUA/MODIS observations.

2.2.1 Satellite data

MODIS and CERES are the key instruments of the AQUA and the TERRA satellite and are important in NASA's Earth Observing System (EOS). The AOD products from MODIS and the radiative flux products at the TOA from CERES can be synergistically used to estimate the $DRFE_{dust}$ directly.

Several algorithms have been developed for MODIS AOD remote-sensing products after MODIS instruments were launched (Remer et al., 2005). Of these algorithms, the Deep Blue algorithm (Hsu et al., 2004) solved the problems in aerosol retrieval by satellite remote-sensing for high reflectance land surface types (such as arid, semi-arid, and desert areas), and retrieved the AOD over high reflectance

land surface types. In this paper, the deep blue AOD (0.55μm) data are used to discriminate the dust storm regions. Since the Sahara Desert and the Taklimakan Desert are free of industrial activities, the major aerosol over the desert areas is dust aerosol, and the anthropogenic and marine aerosols have little contribution to the total AOD, especially during dust storm episodes. Thus, we directly use the AOD retrieved by MODIS to estimate $DRFE_{dust}$ during dust storms in this study. The LSA is also needed both in the satellite-based equi-albedo method and the RTM. The MODIS Collection6 albedo product dataset (MCD43C3) (Schaaf et al., 2011;Schaaf et al., 2002a;Schaaf et al., 2008) provides high-quality land surface reflectance and albedo data over various types of land surfaces by using anisotropy retrievals algorithm (Jin et al., 2003;Liang et al., 2002;Liu et al., 2009;Román et al., 2010). The MCD43C3 product dataset is available from the Land Processes Distributed Active Archive Center (LP DAAC) of NASA. The SW white-sky albedo (WSA) and black-sky albedo (BSA) from the MCD43C3 product are used to get the SW broadband (0.3–5.0 μm) LSA. BSA and WSA mark the extreme cases of completely direct and completely diffuse illumination. Here, the LSA is calculated by interpolating from BSA and WSA (Lewis and Barnsley, 1994;Schaaf et al., 2002b).

The CERES Single Scanner Footprint (SSF) Level 2 instantaneous SW Flux data is available at http://ceres.larc.nasa.gov. The CERES SSF is a unique product for studying the role of clouds, aerosols and radiation in climate. CERES single scanner footprint (SSF) level 2 dataset can provide the radiative flux at the TOA in three broadband channels. The radiative flux derived from CERES is co-located with the MODIS scene. Here the instantaneous SW channel (0.3–5.0 μm) radiative flux at the TOA from CERES SSF level 2 dataset is used. MODIS and CERES are onboard in the same satellite platform (AQUA). The DRE_{dust} and the $DRFE_{dust}$ at the TOA are estimated by synergistically using MODIS and CERES products.

2.2.2 Dust microphysical property data

The Aerosol Robotic Network (AERONET) (Holben et al., 1998) is the largest ground-based network for measuring aerosols with more than 400 sites installed.

The AERONET provides microphysical properties and optical properties of the aerosols at four wavelengths (440, 675, 870, and 1020 nm). The AOD product is directly measured by the sun photometer. The inversion algorithm retrieves the physical properties of aerosols such as volume size

distributions and the complex refractive index, and optical properties such as the SSA and the ASY (Dubovik and King, 2000;Dubovik et al., 2006).

3 $DRFE_{dust}$ estimated based on satellite observations

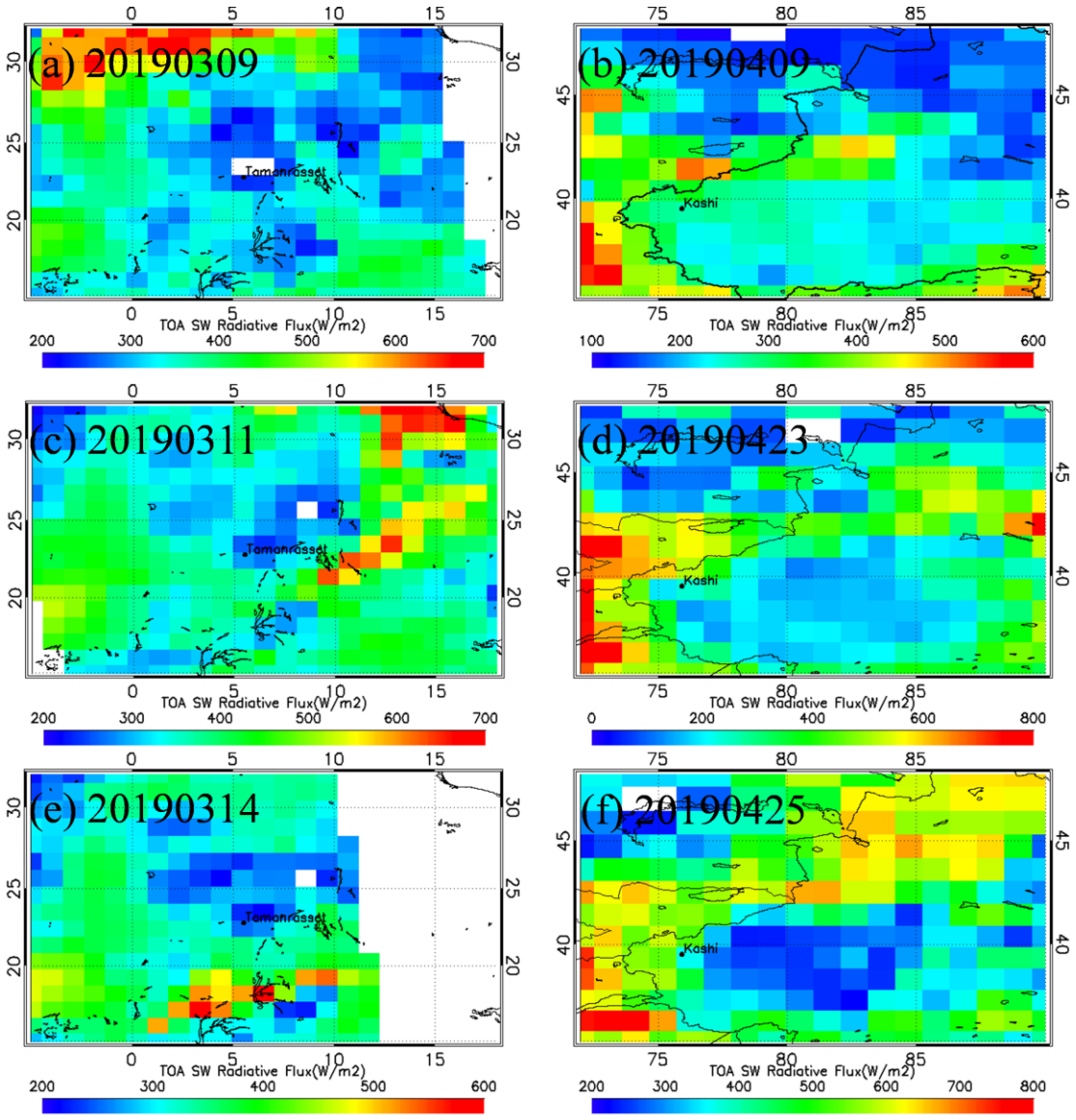

Figure 5: TOA SW radiative flux derived from AQUA/CERES over the Sahara Desert on March 2019 and over the Taklimakan Desert on April 2019.

Figure 5 shows the TOA SW radiative flux measured by CERES over the Sahara Desert in March 2019 and that over the Taklimakan Desert in April 2019 during the dust storm episodes. The TOA SW radiative flux distribution shows the highest value over cloud conditions (the cloud regions can be found from Fig. 4). The values in dust storm regions are higher than those in clear-sky regions. It is due to the SW albedo of the dust aerosols and cloud is higher than the land surface albedo.

As shown in Fig. 3, Fig. 5 and Fig. 6, the spatial resolution of TOA flux from CERES/SSF product is 1 °×1 °, and LSA, SZA, AOD data from satellite have the different spatial resolutions. In order to match up LSA, SZA and AOD data with CERES TOA SW fluxes, we have resampled LSA, SZA and AOD data following the horizontal spatial resolution of CERES SSF products. Following the equi-albedo method (Tian et al., 2019), the F_{clr} and DRE_{dust} over the Sahara Desert and the Taklimakan Desert can be estimated based on the measurements from MODIS and CERES both aboard on the AQUA satellite.

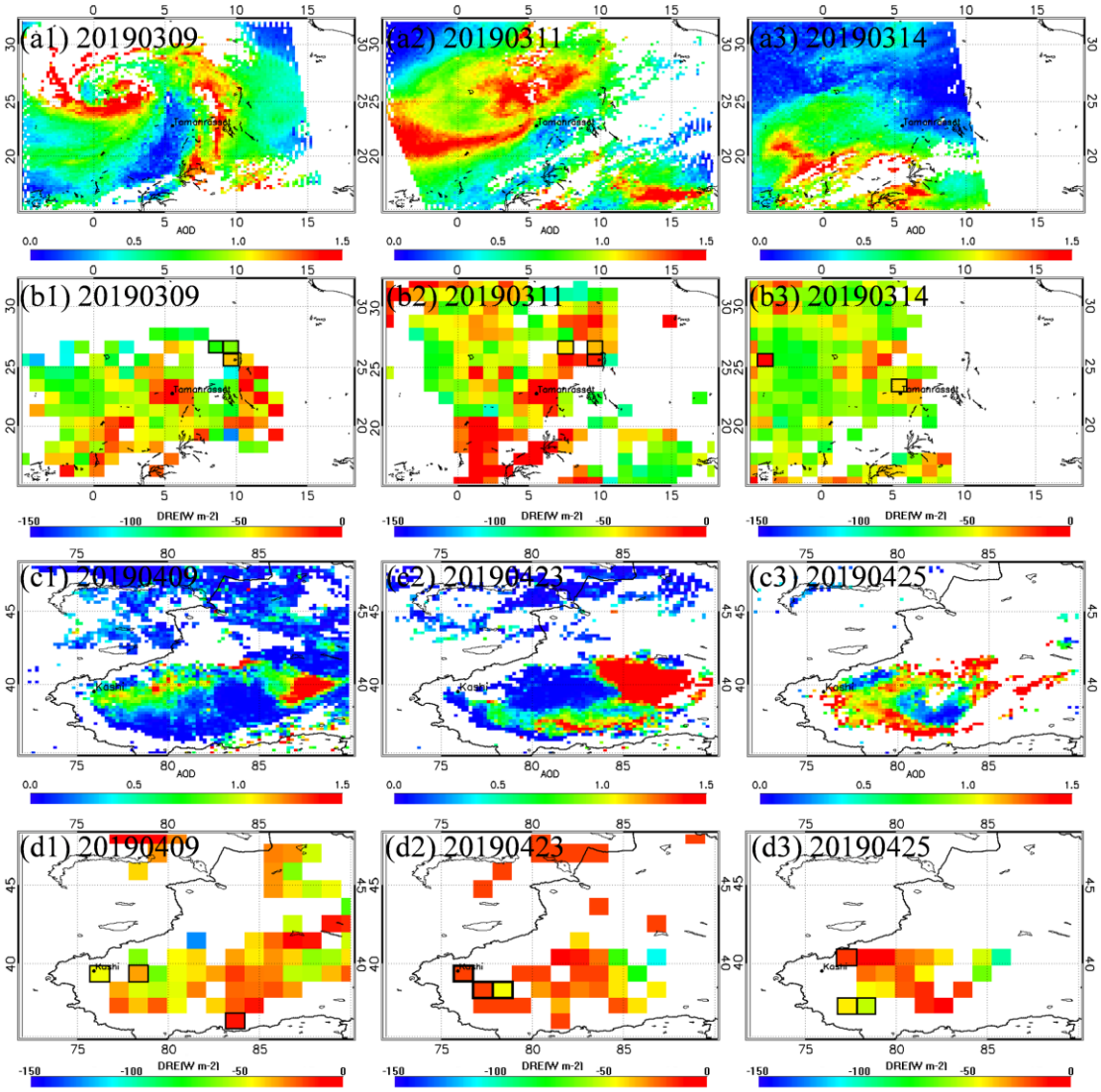

Figure 6: AOD and DRE_{dust} of dust storms over the Sahara Desert in March 2019 and over the Taklimakan Desert in April 2019.

MODIS L2 deep blue AOD products of the dust storm over the Sahara Desert in March 2019 and that over the Taklimakan Desert in April 2019 are shown in Fig. 6(a1)–(a3) and Figs. 6(c1)–(c3),

306 respectively. The missing data are shown in white; the high dust loading regions are shown in red; the
307 low dust loading regions are shown in blue. The AOD distribution maps show that there were heavy
308 dust storms over the Sahara Desert and the Taklimakan Desert with AOD great than 1.0 detected by
309 MODIS.

310 Figs. 6(b1)–(b3) and Figs. 6(d1)–(d3) show the distribution maps of the DRE_{dust} at the TOA. The
311 high dust aerosol loading regions show significant negative radiative forcing. It indicates that the dust
312 aerosol loading is negatively correlated with the DRE_{dust} in these dust storm events. Thus, dust aerosols
313 have a negative radiative effect in the SW spectrum. The distribution maps of the LSA and the SZA
314 (Fig. 3) show that the mean SW LSA measured by MODIS is around 0.18 and the mean SZA is around
315 35 degrees in Tamanrasset and Kashi. The distribution maps also show that the LSA and SZA vary
316 greatly in the same satellite scan image. In our previous study, we found that DRE_{dust} at the TOA was
317 significantly influenced by LSA and SZA (Tian et al., 2019). To avoid the influence of the LSA and
318 SZA in estimating the $DRFE_{dust}$, we estimate $DRFE_{dust}$ using pixels with similar LSAs and SZAs.
319 Furthermore, the values of AOD and cloud could also influence the regions we selected. The deep blue
320 algorithm retrieved AOD has large uncertainties in the small value areas. The cloud-free pixels with
321 AOD great than 0.1, and with the LSA of 0.16–0.20 and the SZA of 32–38 degrees are chosen to
322 estimate the $DRFE_{dust}$. Therefore, only few pixels having similar values of the LSA and the SZA at
323 Tamanrasset and Kashi are picked for estimating the DRE_{dust} and $DRFE_{dust}$ at the TOA. These chosen
324 pixels are surrounded by black border in Figs. 6(b1)–(b3) and Figs. 6(d1)–(d3). The influences of the
325 dust microphysical properties on the $DRFE_{dust}$ are investigated. These pixels of the DRE_{dust} and its
326 co-located AOD values are illustrated in Table 1.

327 **Table 1: DRE_{dust} at the TOA and AOD over the Sahara Desert in March 2019 and that over the**
328 **Taklimakan Desert in April 2019 during the dust storms.**

Regions & Dates \ Properties		AOD	DRE_{dust}
Sahara Desert	20190309	0.92	-41.2
		1.51	-63.7
		1.11	-57.8
		0.31	-15.6
	20190311	0.48	-11.5

		1.41	-43.5
		0.87	-36.7
	20190314	1.14	-44.6
		0.15	-5.8
	20190409	0.31	-12.3
		0.72	-39.5
		0.88	-35.4
	20190423	0.21	-8.3
Taklimakan Desert		0.35	-35.7
		0.11	-4.5
	20190425	0.79	-44.8
		0.98	-52.4
		0.55	-29.1

According to the definition, the $DRFE_{dust}$ represents the DRE_{dust} of per unit AOD during these storms in the dust source regions. Therefore, the $DRFE_{dust}$ can be estimated by fitting the DRE_{dust} and the AOD.

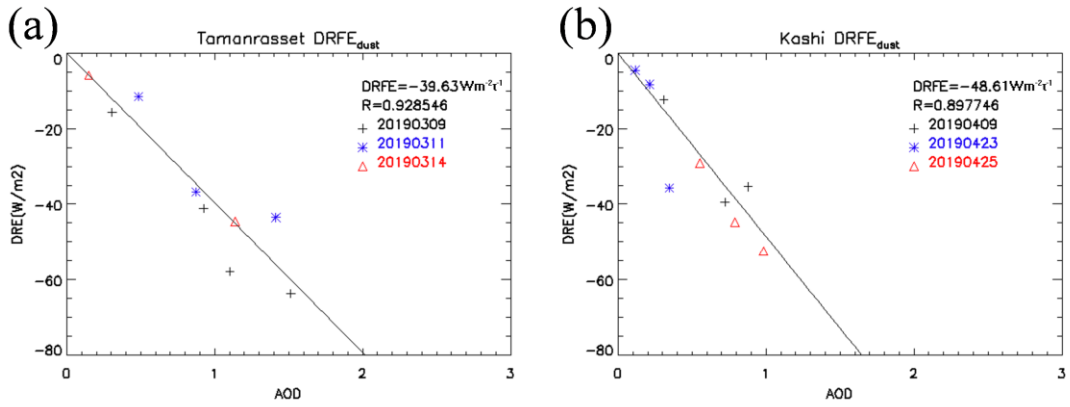

Figure 7: DRE_{dust} in (a) March 2019 over Tamanrasset and (b) April 2019 over Kashi.

The linear relationship between the DRE_{dust} and the AOD (0.55μm) can be found during dust storms around Tamanrasset and Kashi, which is also investigated in previous studies (Kumar et al. 2015; Jose et al. 2016). Then, the $DRFE_{dust}$ can be estimated by regressing the DRE_{dust} and the AOD. In Fig. 7, the mean $DRFE_{dust}$ of the dust storms is -39.6 $Wm^{-2}\tau^{-1}$ over Tamanrasset and -48.6 $Wm^{-2}\tau^{-1}$ over Kashi. The correlation coefficients are high with R = 0.92 in March 2019 over Tamanrasset and R =

0.89 in April 2019 over Kashi. The AOD and DRE_{dust} values are well correlated. Positive dust AOD is associated with negative DRE_{dust}.

The equi-albedo method directly estimates the DRE_{dust} and the $DRFE_{dust}$ based on the satellite observations. Therefore, the accuracy of the results (DRE_{dust} and $DRFE_{dust}$) derived from the equi-albedo method is highly dependent on the accuracy of satellite observations. Therefore, the uncertainties of the $DRFE_{dust}$ derived from the equi-albedo method mainly include the instantaneous SW flux error from CERES measurements, the estimation uncertainties of the F_{clr} over the dust storm region, and the uncertainty in the deep blue AOD product. Besides, according to our sensitivity test in the previous study (Tian et al., 2019), the atmospheric profile, water vapor and height of dust layer have insignificant influence on SW radiative flux at the TOA. It is reasonable to use same water vapor and pre-defined vertical distribution for dust aerosols in one scene of satellite data. However, the assumption of pixels has same water vapor and pre-defined aerosol vertical distribution over one scene of satellite data still cause small uncertainties.

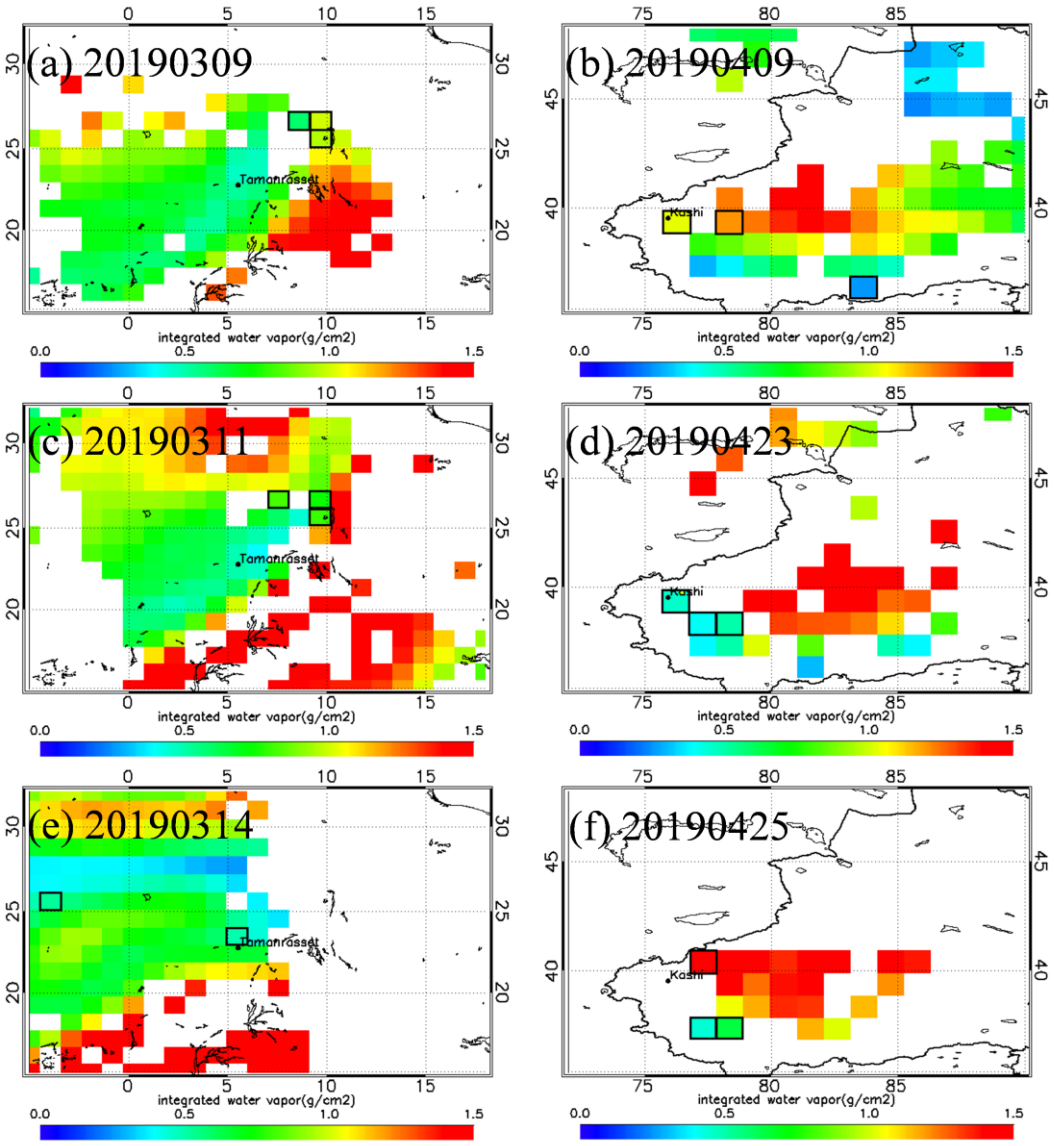

Figure 8: Integrated water vapor (g/cm^2) from European Centre for Medium-range Weather Forecasts (ECMWF) reanalysis dataset over the Sahara Desert in March 2019 and over the Taklimakan Desert in April 2019.

Fig.8 shows the integrated water vapor from ECMWF reanalysis dataset over the Sahara Desert in March 2019 and over the Taklimakan Desert on April 2019. The grids surrounded by black border are the chosen pixels to estimate the $DRFE_{dust}$. The integrated water vapor varies little over different research areas, and the mean differences of chosen pixels are 0.51g/cm^2 and 0.18g/cm^2 over the Sahara Desert and the Taklimakan Desert, respectively. In order to estimate the uncertainties caused by the variation of integrated water vapor over chosen pixels, we have calculated the SW radiative flux at the TOA under different integrated water vapor based on the SBDART model.

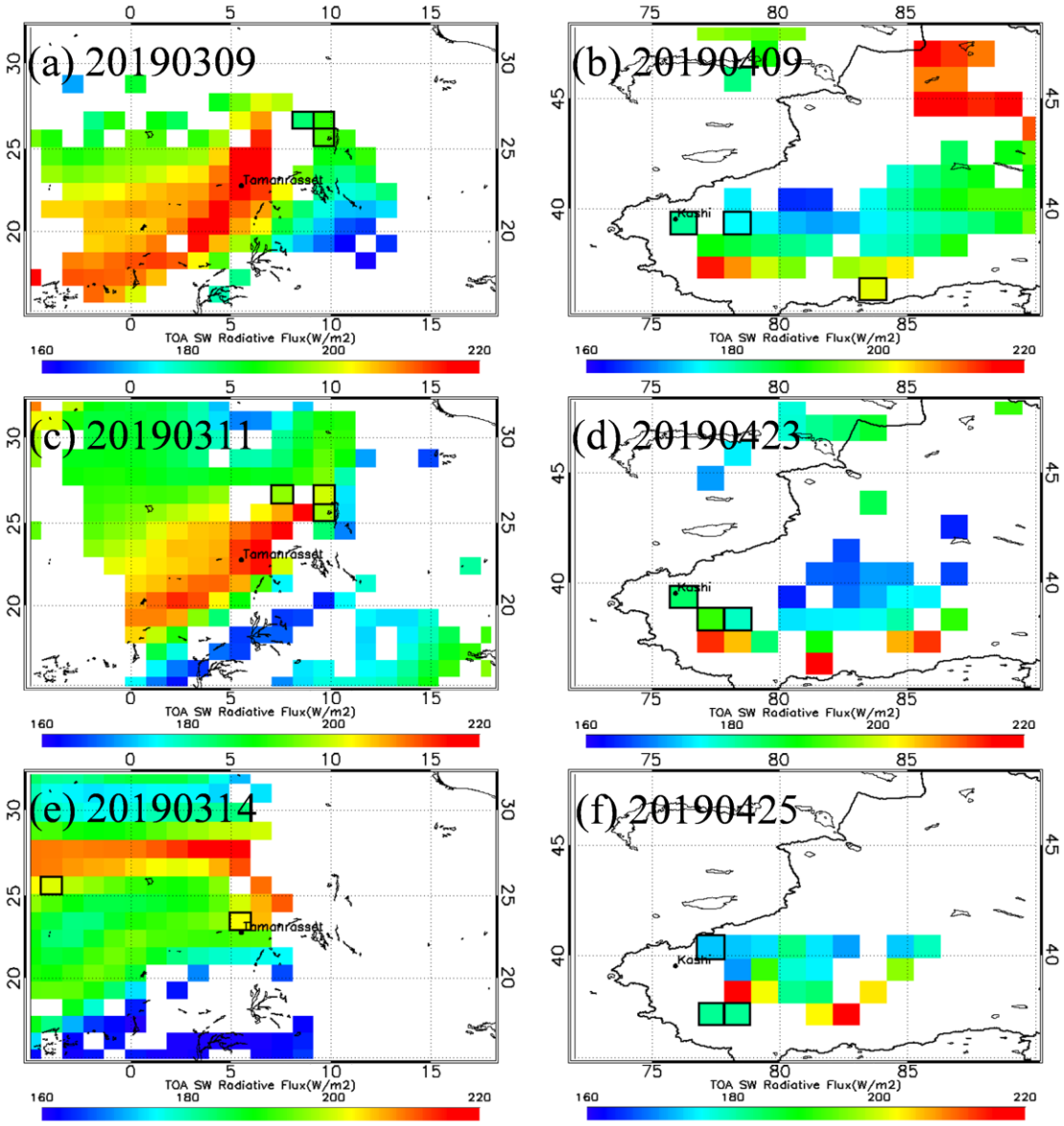

Figure 9: SBDART simulated clear-sky TOA radiative flux by using integrated water vapor (g/cm^2) from ECMWF reanalysis dataset over the Sahara Desert in March 2019 and over the Taklimakan Desert in April 2019.

Fig. 9 shows the SBDART simulated clear-sky TOA radiative flux by using the integrated water vapor from ECMWF reanalysis dataset over the Sahara Desert in March 2019 and over the Taklimakan Desert in April 2019, and the grids surrounded by black border are the chosen pixels to derive the $DRFE_{dust}$. The regional mean differences of TOA radiative flux are 2.21% and 0.85% over the Sahara Desert and the Taklimakan Desert, respectively. This indicates the variation of integrated water vapor cloud cause uncertainties of TOA radiative flux by 2.21% and 0.85% over the Sahara Desert and the

Taklimakan Desert.

For the assumption of vertical profile for dust aerosols, we have also tested the sensitivity of radiative flux at the TOA to various heights of dust layer with the SBDART model.

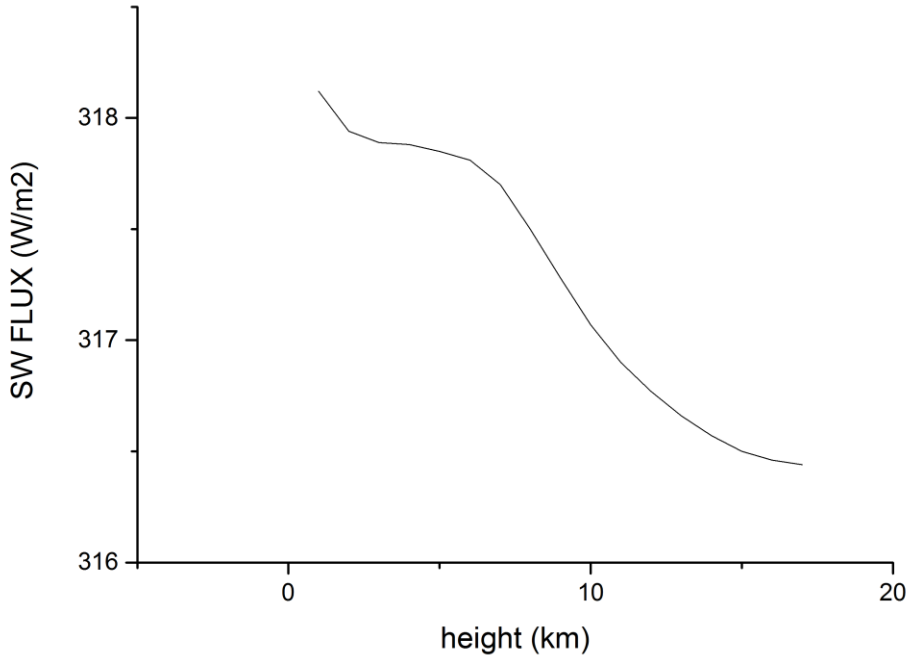

Figure 10: The sensitivity test of SW radiative flux at the TOA to various heights of dust layer.

As shown in Fig. 10, the SW radiative flux at the TOA decreases with the increase of the height of dust layer. However, the contents of the SW radiative flux change little with the increase of the height of dust layer (within 1.5Wm^{-2}, 0.47%).

According to our previous study (Tian et al., 2019), the instantaneous SW flux error from CERES measurements is about 3.13%, the estimation uncertainty of the F_{clr} is 3.15%, the uncertainty of the deep blue AOD retrieved by MODIS is about 15% (Sayer et al., 2014). Over one scene of satellite data, the uncertainties of using same water vapor in Kashi and Tamanrasset are 2.21% and 0.85%, respectively, and the uncertainty caused by pre-defined aerosol vertical distribution is also estimated, which is about 0.47%. Then, the total uncertainties of the $\mathrm{DRFE}_{\mathrm{dust}}$ can be calculated by the equation Eq. (3) (Zhang et al., 2005).

$$U_t = \exp[\sum(logU_s)^2]^{1/2} \quad (3).$$

U_s is the synthetical uncertainty factor of each source of the uncertainty (including the instantaneous SW flux error from CERES measurements, the estimation uncertainty of the F_{clr}, and the

uncertainty of the deep blue AOD retrieved by MODIS). U_t is the total uncertainty of the $DRFE_{dust}$, which is 25.37% and 28.19% (10.0 $Wm^{-2}\tau^{-1}$ and 13.7 $Wm^{-2}\tau^{-1}$) in Tamanrasset and Kashi, respectively. Therefore, the $DRFE_{dust}$ are -39.6 ± 10.0 $Wm^{-2}\tau^{-1}$ in March 2019 over Tamanrasset and -48.6 ± 13.7 $Wm^{-2}\tau^{-1}$ in April 2019 over Kashi.

4 Deriving $DRFE_{dust}$ from the RTM simulations

4.1 Dust microphysical properties

The inversion of sun-photometry optical data to obtain particle microphysical properties has been done through numerous approaches. Currently, the AERONET inversion algorithm makes use of direct sun and sky radiance measurements (Dubovik et al., 2006;Dubovik and King, 2000).

The focuses of this paper are the differences in the dust microphysical properties from different dust source regions and the impacts of the dust microphysical properties on the $DRFE_{dust}$ simulation. As important parameters concerning the radiative impacts, the volume size distribution and the refractive index of the dust aerosol are compared in the dust storms over Tamanrasset and Kashi detected by MODIS.

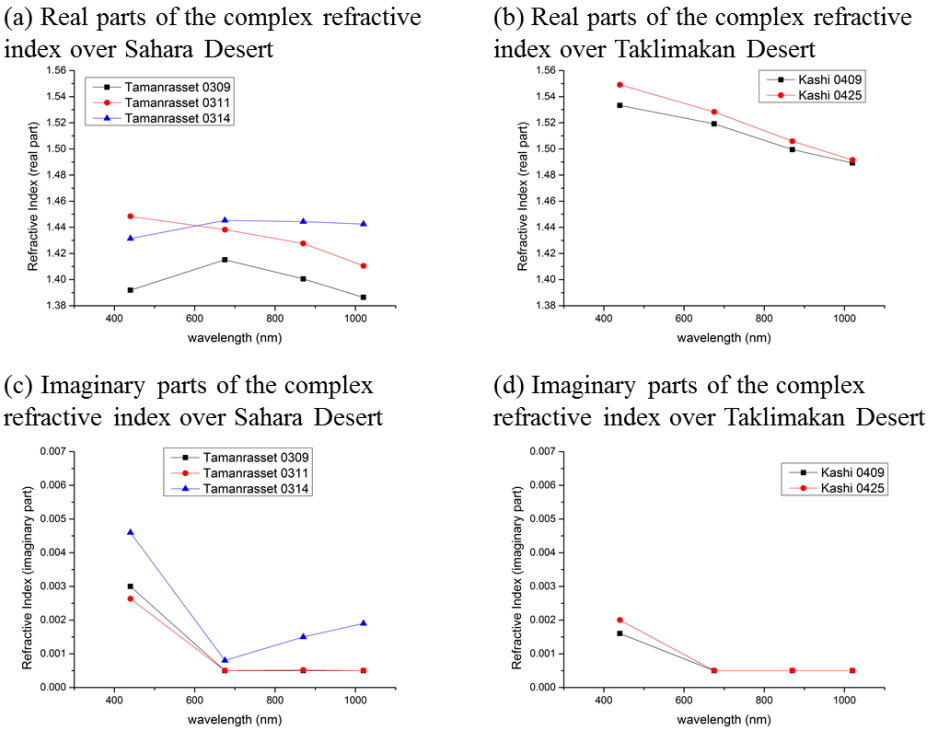

Figure 11: Real and imaginary parts of the dust complex refractive index from the Sahara Desert and the Taklimakan Desert.

The refractive index is a measurement of the aerosol refraction and absorption efficiency. Aerosols with high real parts of the complex refractive index values are indicated to be scattering types. Conversely, aerosols with high imaginary parts are indicated to be absorbing types (Zhang et al., 2006). Figure 11 shows the real and imaginary parts of the dust complex refractive index from the Taklimakan Desert and the Sahara Desert during the dust storms. In Fig. 11, dust aerosols from the Taklimakan Desert have higher real parts (Fig. 11 (b)) and lower imaginary parts (Fig. 11 (d)) than the Sahara Desert (Fig. 11 (a) and Fig. 11 (c)), showing that the dust aerosols from the Taklimakan Desert have stronger scattering effects.

Figure 12 illustrates the variation of the dust aerosol size distribution during the dust storms over Tamanrasset in March 2019 and over Kashi in April 2019. Most maximum dust aerosol size distribution peaks at the radius of 1.71μm in Tamanrasset and 2.24μm in Kashi. Moreover, the peak values are higher in Kashi. It is indicated that the dust storm was stronger in Kashi in April 2019, and the coarse mode aerosol particles increased in particle volume compared with those in the dust storm in Tamanrasset in March 2019.

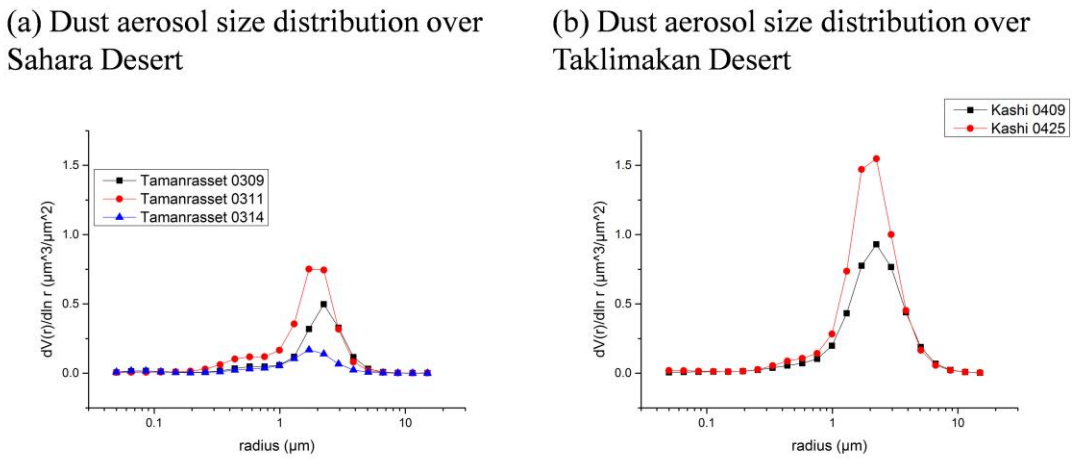

Figure 12: Dust aerosol size distribution over (a) the Sahara Desert and (b) the Taklimakan Desert.

4.2 Dust optical properties

The dust optical properties can be calculated by synergistically using the real and imaginary parts of the dust complex refractive index and the dust aerosol size distribution.

The SSA and the ASY are two key parameters determining the DRE_{dust} and the $DRFE_{dust}$. Accurate measurements of the SSA and the ASY are important for the assessment of the direct effect of aerosols on climate (Qie et al., 2019). The dust aerosol optical properties are calculated by using the Mie theory,

the T-matrix method, and the AERONET inversion products (Dubovik and King, 2000;Dubovik et al., 2006).

The SSA is presented as the ratio between the aerosol scattering and extinction coefficients. The dust SSA describes the scattering properties of the dust aerosols. The SSA can largely determine the magnitudes and signs of the DRE_{dust} and the $DRFE_{dust}$. Strongly scattering dust aerosols (i.e., SSA = 1) always cause negative DRE_{dust}. By contrast, low SSA aerosols often cause positive DRE_{dust}, especially over high LSA regions as the light absorbed by the aerosols can reduce the cooling effect. The size distribution and the complex refractive index can codetermine the magnitude of the SSA.

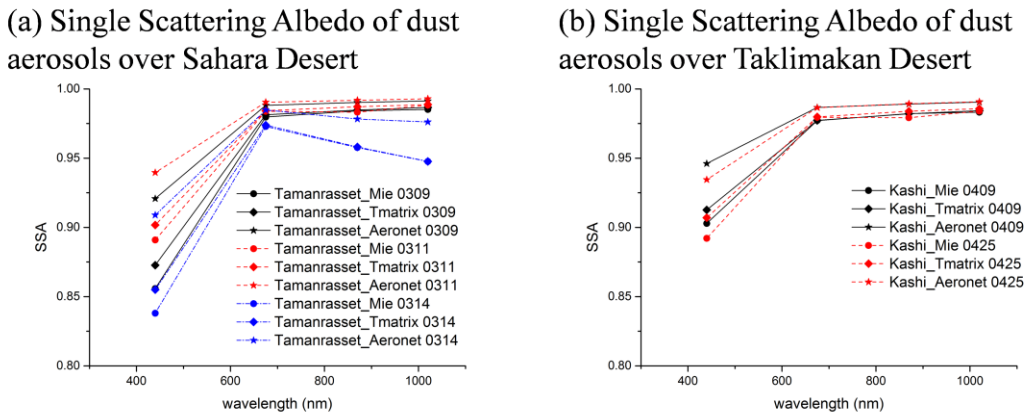

Figure 13: Single scattering albedo from (a) the Sahara Desert and (b) the Taklimakan Desert.

Figure 13 shows the variabilities of the dust aerosol SSA between different dust source regions and different calculation methods. In Fig. 13, the maximum SSA value mostly occurs at the wavelength of 1020 nm, which indicates that the SSA is dependent on wavelength. Moreover, dust aerosols from the Taklimakan Desert (Kashi) in the figure have higher SSA value using both the Mie theory and the T-matrix method. The higher value of SSA shows that dust aerosol particles scatter more predominantly and strongly in the Taklimakan Desert (Kashi), which may cause more significant negative radiative forcing than the dust aerosols from the Sahara Desert (Tamanrasset).

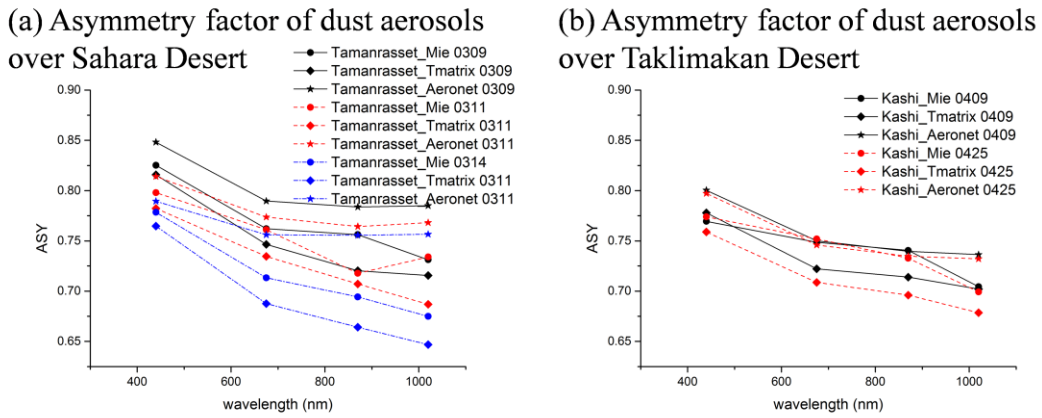

Figure 14: Asymmetry factor in (a) the Sahara Desert and (b) the Taklimakan Desert.

The ASY indicates the relative strength of the forward scattering, which determines the integrated fractions of the energy that scatter backward and forward. The dust aerosol particles with sharp peaks in the forward direction (0 ° scattering angle) have positive ASY. The ASY value increases with the particle size.

The ASY in Fig. 14 shows marked spectral variation with higher values at shorter wavelengths. It can be found that the dust aerosols from the Sahara Desert (Tamanrasset) have higher values of the ASY than those from the Taklimakan Desert (Kashi) in both the Mie theory and the T-matrix method. The stronger backward scattered energy may cause higher negative radiative forcing in the Taklimakan Desert (Kashi) at the TOA.

According to the analyses of the microphysical properties and the optical properties, the dust aerosols from the Taklimakan Desert (Kashi) scatter strongly. The negative $DRFE_{dust}$ from the Taklimakan Desert (Kashi) should be more significant than those from the Sahara Desert (Tamanrasset). The results are in good agreement with those estimated by the satellite observations.

4.3 $DRFE_{dust}$ derived from the RTM simulations

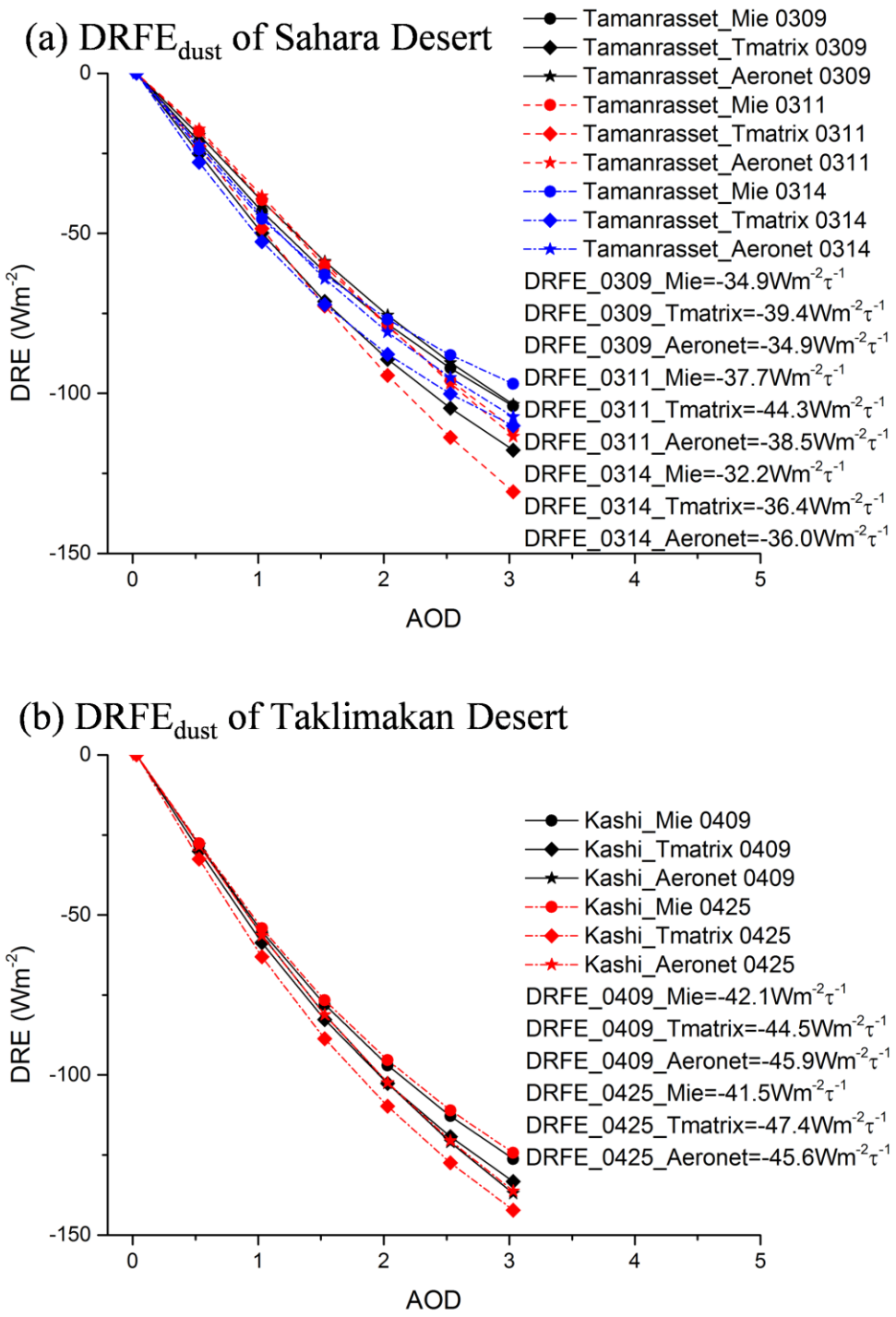

Figure 15: $DRFE_{dust}$ simulated by the SBDART in (a) Tamanrasset and (b) Kashi.

The $DRFE_{dust}$ estimated directly by the satellite observation is compared with that simulated by the SBDART to verify the reliability. As shown in Fig. 15, with higher aerosol scattering (higher SSA in Fig. 13) and higher backward scattering (lower ASY in Fig. 14), the negative $DRFE_{dust}$ from Kashi is

more significant. The mean $DRFE_{dust}$ from Tamanrasset is -37.1 W m^{-2} τ^{-1}. The dust aerosols from Kashi have stronger cooling effects than those from Tamanrasset, in which the mean $DRFE_{dust}$ is -44.5 W m^{-2} τ^{-1}. The results are in good agreement with those estimated by the satellite observations. The $DRFE_{dust}$ estimated by the dust optical properties derived from the T-matrix method and the AERONET is closer to those estimated by the satellite observations, which indicates that most dust aerosols are non-spherical in the natural environment.

The results also show that the dust microphysical properties can significantly influence the $DRFE_{dust}$. The mean difference of the $DRFE_{dust}$ between Tamanrasset and Kashi (difference between the mean $DRFE_{dust}$ in Tamanrasset and in Kashi) is 18.14% (7.4 W m^{-2} τ^{-1}). Even for the same size distributions and the complex refractive index of dust aerosol, the $DRFE_{dust}$ varies significantly according to whether the dust particles are considered spherical or non-spherical in different methods. For the differences of the $DRFE_{dust}$ estimated using different methods, the mean standard deviations are 7.6% (2.8 W m^{-2} τ^{-1}) in Tamanrasset and 6.8% (3.0 W m^{-2} τ^{-1}) in Kashi. Moreover, Li et al. (2020) pointed out that the atmospheric profile, LSA and SZA, can also influence the simulation of the instantaneous $DRFE_{dust}$, which agrees with our previous study (Tian et al., 2019). Additionally, it is difficult for climate models or in-situ measurements to get the real distribution of the aerosol properties at a large spatial extent. Also, it is hard to evaluate the uncertainties in radiative transfer simulations. It can cause significant errors in evaluating the modulating effects of the mineral dust aerosols on climate (Huang et al., 2009;Li et al., 2020).

5 $DRFE_{dust}$ in the satellite-based observation and the simulation of the RTM

According to the analyses of the dust aerosol microphysical properties and optical properties, the dust aerosols from the Taklimakan Desert (Kashi) should scatter strongly. The RTM simulation results are in good agreement with the results estimated by the satellite observation. Previous studies also estimated the $DRFE_{dust}$ in the Sahara Desert and the Taklimakan Desert (Li et al., 2020;Li et al., 2004;Garc á et al., 2012;Xia and Zong, 2009), which validate our results.

Table 2: SW $DRFE_{dust}$ from different studies.

Dust source regions	Research	Model/Method	$DRFE_{dust}$ ($Wm^{-2}\tau^{-1}$)	Description
Sahara	Li et al (2004)	Satellite+SBD	-35 ±3 (summer)	Binned mean

Desert		ART	-26±3 (winter)	fitting TOA diurnal mean $DRFE_{dust}$ over the Atlantic Ocean near the African coast.
	This paper	Satellite	-39.6±10.0 (Satellite)	
		Satellite+SBDART	-32.2 ~ -44.3 (SBDART)	
	Li et al (2020)	Ground+SBDART	-45~-50	Instantaneous $DRFE_{dust}$.
	Xia and Zong (2009)	Satellite + SBDART	-48.1	Instantaneous $DRFE_{dust}$ at about 05:00 UTC.
	This paper	Satellite	-48.6±13.7 (Satellite)	
		Satellite+SBDART	-41.5 ~ -47.4 (SBDART)	

Table 2 illustrates the SW $DRFE_{dust}$ of the Sahara Desert and the Taklimakan Desert in previous studies. Li et al. (2004) estimated the diurnal mean $DRFE_{dust}$ at the TOA (-35 ± 3 W m^{-2} τ^{-1} in summer; -26 ± 3 W m^{-2} τ^{-1} in winter) over the Atlantic Ocean near the African coast. The results indicated that lower uncertainties are derived from the standard deviation of the best-fit curve around the observed points due to the binned mean fitting. For the Taklimakan Desert, Li et al. (2020) estimated the instantaneous SW $DRFE_{dust}$ at the TOA of Kashi on April 2019. In this paper, the $DRFE_{dust}$ of the Taklimakan Desert is estimated with the same dust properties referring to the works of Li et al. (2020). Furthermore, Xia and Zong (2009) used both the satellite data and the SBDART model to represent the instantaneous (about 05:00 UTC) SW $DRFE_{dust}$, which is -48.1 W m^{-2} τ^{-1} at the TOA(Xia and Zong, 2009). Through comparison, it is found that the satellite-based equi-albedo method and the SBDART model-derived SW $DRFE_{dust}$ are -39.6 ± 10.0 W m^{-2} τ^{-1} and -32.2 to -44.3 W m^{-2} τ^{-1} at the TOA over the Sahara Desert, respectively, which are -48.6 ± 13.7 W m^{-2} τ^{-1} and -41.5 to -47.4 W m^{-2} τ^{-1} at the TOA over the Taklimakan Desert, respectively. The methods and results in these studies are comparable despite the differences. The results show that the negative $DRFE_{dust}$ from the Taklimakan Desert is more significant than those from the Sahara Desert. As the SZA and LSA variations are considered in these studies, the results in this paper are reasonable and reliable. The compared results show that the $DRFE_{dust}$ derived from the satellite-based equi-albedo method is closer to that in previous

studies. The $DRFE_{dust}$ estimated by the satellite-based equi-albedo method is obtained without the dust microphysical properties being assumed. The uncertainties are mostly caused by observation errors. Therefore, the uncertainties can be evaluated more reasonably. It provides a direct way to validate the DRE_{dust} and the $DRFE_{dust}$.

6 Discussion and conclusions

This study analyzes the differences in the dust microphysical properties and the $DRFE_{dust}$ over the Taklimakan Desert and the Sahara Desert during dust storms. The satellite-based equi-albedo method and the RTM are both used to estimate the $DRFE_{dust}$ in this study. By comparing the results from different methods and dust source regions, the $DRFE_{dust}$ differences caused by dust microphysical properties and particle shapes are discussed.

The results show that the dust aerosols from the Taklimakan Desert have higher aerosol scattering (higher SSA) and backward scattering (lower ASY), and it causes more significant negative $DRFE_{dust}$ (-48.6 ± 13.7 W m^{-2} τ^{-1} by the satellite; -41.5 to -47.4 W m^{-2} τ^{-1} by the SBDART) than that in the Sahara Desert (-39.6 ± 10.0 W m^{-2} τ^{-1} by the satellite; -32.2 to -44.3 W m^{-2} τ^{-1} by the SBDART). It is indicated that the dust microphysical properties and particle shapes can significantly influence on the $DRFE_{dust}$. The information on the accurate dust microphysical properties and dust origins is highly required in the $DRFE_{dust}$ simulation. The scant measurements on dust microphysical properties can cause large uncertainties in simulating the $DRFE_{dust}$. Previous studies proved that the results in this paper are reasonable and reliable. The $DRFE_{dust}$ derived from the satellite-based equi-albedo method is close to the results in previous studies.

However, there are still uncertainties in the simulation of the $DRFE_{dust}$. In contrast, the $DRFE_{dust}$ can be estimated directly from the satellite observation using the equi-albedo method without any assumptions of the microphysical properties of dust aerosols. It has unique advantages in estimating the $DRFE_{dust}$. Also, it can validate the DRE_{dust} and the $DRFE_{dust}$ derived from the numerical models more directly.

Data availability

The CERES data can be accessed from the Atmospheric Sciences Data Center of NASA Langley Research Center (https://ceres.larc.nasa.gov/order_data.php). The AQUA/MODIS aerosol Products (MYD04_L2) can be accessed from the NASA Level-1 and Atmosphere Archive and Distribution System (LAADS) Distributed Active Archive Center (DAAC) website (https://ladsweb.modaps.eosdis.nasa.gov/). The MODIS albedo products (MCD43C3 Version 6) can be accessed from the NASA LP DAAC website (https://lpdaac.usgs.gov/tools/data-pool/). The AERONET data were obtained from the AERONET website (http://aeronet.gsfc.nasa.gov).

Author contributions

PZ and LC designed the study, and LT performed the study with suggestions from PZ and LC. LB improved the scattering calculating method of dust particles. Both authors contributed to the writing of this article.

Competing interests

The authors declare that they have no conflict of interest.

Special issue statement

This article is part of the special issue “Satellite and ground-based remote sensing of aerosol optical, physical, and chemical properties over China”. It is not associated with a conference.

Acknowledgments

We acknowledge the groups of MODIS, CERES, ECMWF, AERONET and GISS, for providing the AOD, LSA, integrated water vapor, aerosol microphysical, optical properties products and T-matrix code. We also thank the SBDART group for making SBDART available. We thank Nanjing Hurricane Translation for reviewing the English language quality of this paper.

Financial support

This work was funded by the National Key R&D Program of China (grant number 2018YFB0504900 and 2018YFB0504905), National Natural Science Foundation (grant number 41675036).

References

Anderson, T. L., Charlson, R. J., Bellouin, N., Boucher, O., Chin, M., Christopher, S. A., Haywood, J., Kaufman, Y. J., Kinne, S., Ogren, J. A., Remer, L. A., Takemura, T., Tanré, D., Torres, O., Trepte, C. R., Wielicki, B. A., Winker, D. M., and Yu, H.: An "A-Train" Strategy for Quantifying Direct Climate Forcing by Anthropogenic Aerosols, Bulletin of the American Meteorological Society, 86, 1795-1810, 10.1175/bams-86-12-1795, 2005.

Bi, J., Shi, J., Xie, Y., Liu, Y., Takamura, T., and Khatri, P.: Dust Aerosol Characteristics and Shortwave Radiative Impact at a Gobi Desert of Northwest China during the Spring of 2012, Journal of the Meteorological Society of Japan. Ser. II, 92A, 33-56, 10.2151/jmsj.2014-A03, 2014.

Bi, L., Ding, S., Zong, R., and Yi, B.: Examining Asian dust refractive indices for brightness temperature simulations in the 650–1135 cm−1 spectral range, Journal of Quantitative Spectroscopy and Radiative Transfer, 247, 106945, https://doi.org/10.1016/j.jqsrt.2020.106945, 2020.

Borghese, F., Denti, P., Saija, R., and Iatì, M. A.: Optical trapping of nonspherical particles in the T-matrix formalism, Opt. Express, 15, 11984-11998, 10.1364/OE.15.011984, 2007.

Che, H., Zhang, X., Alfraro, S., Chatenet, B., Gomes, L., and Zhao, J.: Aerosol optical properties and its radiative forcing over Yulin, China in 2001 and 2002, Advances in Atmospheric Sciences, 26, 564-576, 10.1007/s00376-009-0564-4, 2009.

Che, H., Wang, Y., Sun, J., Zhang, X., Zhang, X., and Guo, J.: Variation of Aerosol Optical Properties over Taklimakan Desert of China, Aerosol and Air Quality Research, 13, 777-785, 10.4209/aaqr.2012.07.0200, 2012.

Chen, L., Shi, G., Qin, S., Yang, S., and Zhang, P.: Direct radiative forcing of anthropogenic aerosols over oceans from satellite observations, Advances in Atmospheric Sciences, 28, 973-984, 10.1007/s00376-010-9210-4, 2011.

586 Christopher, S. A., Chou, J., Zhang, J., Li, X., Berendes, T. A., and Welch, R. M.: Shortwave direct
587 radiative forcing of biomass burning aerosols estimated using VIRS and CERES data, Geophysical
588 Research Letters, 27, 2197-2200, 10.1029/1999gl010923, 2000.
589 Chylek, P., Grams, G., and Pinnick, R.: Light Scattering by Nonspherical Particles, 82, 1977.
590 Colarco, P. R., Nowottnick, E. P., Randles, C. A., Yi, B., Yang, P., Kim, K.-M., Smith, J. A., and
591 Bardeen, C. G.: Impact of radiatively interactive dust aerosols in the NASA GEOS-5 climate model:
592 Sensitivity to dust particle shape and refractive index, Journal of Geophysical Research: Atmospheres,
593 119, 753-786, 10.1002/2013jd020046, 2014.
594 Di Biagio, C., di Sarra, A., Eriksen, P., Ascanius, S. E., Muscari, G., and Holben, B.: Effect of surface
595 albedo, water vapour, and atmospheric aerosols on the cloud-free shortwave radiative budget in the
596 Arctic, Climate Dynamics, 39, 953-969, 10.1007/s00382-011-1280-1, 2012.
597 Di Biagio, C., Boucher, H., Caquineau, S., Chevaillier, S., Cuesta, J., and Formenti, P.: Variability of the
598 infrared complex refractive index of African mineral dust: Experimental estimation and implications for
599 radiative transfer and satellite remote sensing, Atmospheric Chemistry and Physics, 14,
600 10.5194/acp-14-11093-2014, 2014a.
601 Di Biagio, C., Formenti, P., Styler, S. A., Pangui, E., and Doussin, J.-F.: Laboratory chamber
602 measurements of the longwave extinction spectra and complex refractive indices of African and Asian
603 mineral dust, Geophysical Research Letters, 41, 10.1002/2014GL060213, 2014b.
604 Di Biagio, C., Formenti, P., Balkanski, Y., Caponi, L., Cazaunau, M., Pangui, E., Journet, E., Nowak, S.,
605 Caquineau, S., Andreae, M. O., Kandler, K., Saeed, T., Piketh, S., Seibert, D., Williams, E., and Doussin,
606 J. F.: Global scale variability of the mineral dust long-wave refractive index: a new dataset of in situ
607 measurements for climate modeling and remote sensing, Atmos. Chem. Phys., 17, 1901-1929,
608 10.5194/acp-17-1901-2017, 2017.
609 Dubovik, O., and King, M. D.: A flexible inversion algorithm for retrieval of aerosol optical properties
610 from Sun and sky radiance measurements, Journal of Geophysical Research: Atmospheres, 105,
611 20673-20696, 10.1029/2000jd900282, 2000.
612 Dubovik, O., Sinyuk, A., Lapyonok, T., Holben, B. N., Mishchenko, M., Yang, P., Eck, T. F., Volten, H.,
613 Muñoz, O., Veihelmann, B., van der Zande, W. J., Leon, J.-F., Sorokin, M., and Slutsker, I.: Application
614 of spheroid models to account for aerosol particle nonsphericity in remote sensing of desert dust, Journal
615 of Geophysical Research: Atmospheres, 111, 10.1029/2005jd006619, 2006.

Gao, Y., and Anderson, J. R.: Characteristics of Chinese aerosols determined by individual-particle analysis, Journal of Geophysical Research: Atmospheres, 106, 18037-18045, 10.1029/2000jd900725, 2001.

García, O. E., Díaz, A. M., Expósito, F. J., Díaz, J. P., Dubovik, O., Dubuisson, P., Roger, J.-C., Eck, T. F., Sinyuk, A., Derimian, Y., Dutton, E. G., Schafer, J. S., Holben, B. N., and García, C. A.: Validation of AERONET estimates of atmospheric solar fluxes and aerosol radiative forcing by ground-based broadband measurements, Journal of Geophysical Research: Atmospheres, 113, 10.1029/2008jd010211, 2008.

García, O. E., Díaz, J. P., Expósito, F. J., Díaz, A. M., Dubovik, O., Derimian, Y., Dubuisson, P., and Roger, J. C.: Shortwave radiative forcing and efficiency of key aerosol types using AERONET data, Atmos. Chem. Phys., 12, 5129-5145, 10.5194/acp-12-5129-2012, 2012.

Garrett, T. J., and Zhao, C.: Increased Arctic cloud longwave emissivity associated with pollution from mid-latitudes, Nature, 440, 787-789, 10.1038/nature04636, 2006.

Gouesbet, G., and Gréhan, G.: Generalized Lorenz-Mie Theories, 2011.

Guirado-Fuentes, C., Cuevas, E., Cachorro, V., Toledano, C., Alonso-Pérez, S., Bustos, J., Basart, S., Romero, P., Camino, C., Mimouni, M., Zeudmi, L., Goloub, P., Baldasano, J., and Frutos Baraja, A.: Aerosol characterization at the Saharan AERONET site Tamanrasset, Atmospheric Chemistry and Physics, 14, 11753-11773, 10.5194/acp-14-11753-2014, 2014.

Holben, B. N., Eck, T. F., Slutsker, I., Tanré, D., Buis, J. P., Setzer, A., Vermote, E., Reagan, J. A., Kaufman, Y. J., Nakajima, T., Lavenu, F., Jankowiak, I., and Smirnov, A.: AERONET—A Federated Instrument Network and Data Archive for Aerosol Characterization, Remote Sensing of Environment, 66, 1-16, https://doi.org/10.1016/S0034-4257(98)00031-5, 1998.

Hsu, N. C., Tsay, S. C., King, M. D., and Herman, J. R.: Aerosol properties over bright-reflecting source regions, IEEE Transactions on Geoscience & Remote Sensing, 42, 557-569, 2004.

Huang, J., Fu, Q., Su, J., and Tang, Q.: Taklimakan dust aerosol radiative heating derived from CALIPSO observations using the Fu-Liou radiation model with CERES constraints, Atmospheric Chemistry and Physics Discussions, 2009.

Huang, J., Wang, T., Wang, W., Li, Z., and Yan, H.: Climate effects of dust aerosols over East Asian arid and semiarid regions, Journal of Geophysical Research: Atmospheres, 119, 11,398-311,416, 10.1002/2014jd021796, 2014.

Huneeus, N., Chevallier, F., and Boucher, O.: Estimating aerosol emissions by assimilating observed aerosol optical depth in a global aerosol model, Atmospheric Chemistry & Physics, 12, 4585-4606, 10.5194/acp-12-4585-2012, 2012.

Iftikhar, M., Alam, K., Sorooshian, A., Syed, W. A., Bibi, S., and Bibi, H.: Contrasting aerosol optical and radiative properties between dust and urban haze episodes in megacities of Pakistan, Atmospheric Environment, 173, 157-172, https://doi.org/10.1016/j.atmosenv.2017.11.011, 2018.

Jin, Y., Schaaf, C. B., Woodcock, C. E., Gao, F., Li, X., Strahler, A. H., Lucht, W., and Liang, S.: Consistency of MODIS surface bidirectional reflectance distribution function and albedo retrievals: 2. Validation, Journal of Geophysical Research: Atmospheres, 108, 10.1029/2002jd002804, 2003.

Kalashnikova, O. V., and Sokolik, I. N.: Modeling the radiative properties of nonspherical soil-derived mineral aerosols, Journal of Quantitative Spectroscopy and Radiative Transfer, 87, 137-166, https://doi.org/10.1016/j.jqsrt.2003.12.026, 2004.

Lewis, P., and Barnsley, M.: Influence of the sky radiance distribution on various formulations of the Earth surface albedo, Proc. Conf. Phys. Meas. Sign. Remote Sens., 1994.

Li, F., Vogelmann, A. M., and Ramanathan, V.: Saharan Dust Aerosol Radiative Forcing Measured from Space, Journal of Climate, 17, 2558-2571, 10.1175/1520-0442(2004)017<2558:SDARFM>2.0.CO;2, 2004.

Li, L., Li, Z., Chang, W., Ou, Y., Goloub, P., Li, C., Li, K., Hu, Q., Wang, J., and Wendisch, M.: Solar radiative forcing of aerosol particles near the Taklimakan desert during the Dust Aerosol Observation-Kashi campaign in Spring 2019, Atmos. Chem. Phys. Discuss., 2020, 1-29, 10.5194/acp-2020-60, 2020.

Li, Z. Q., Xu, H., Li, K. T., Li, D. H., Xie, Y. S., Li, L., Zhang, Y., Gu, X. F., Zhao, W., Tian, Q. J., Deng, R. R., Su, X. L., Huang, B., Qiao, Y. L., Cui, W. Y., Hu, Y., Gong, C. L., Wang, Y. Q., Wang, X. F., Wang, J. P., Du, W. B., Pan, Z. Q., Li, Z. Z., and Bu, D.: Comprehensive Study of Optical, Physical, Chemical, and Radiative Properties of Total Columnar Atmospheric Aerosols over China: An Overview of Sun–Sky Radiometer Observation Network (SONET) Measurements, Bulletin of the American Meteorological Society, 99, 739-755, 10.1175/bams-d-17-0133.1, 2018.

Liang, S., Fang, H., Chen, M., Shuey, C. J., Walthall, C., Daughtry, C., Morisette, J., Schaaf, C., and Strahler, A.: Validating MODIS land surface reflectance and albedo products: methods and preliminary

675 results, Remote Sensing of Environment, 83, 149-162, https://doi.org/10.1016/S0034-4257(02)00092-5,
676 2002.
677 Liu, J., Schaaf, C., Strahler, A., Jiao, Z., Shuai, Y., Zhang, Q., Roman, M., Augustine, J. A., and Dutton,
678 E. G.: Validation of Moderate Resolution Imaging Spectroradiometer (MODIS) albedo retrieval
679 algorithm: Dependence of albedo on solar zenith angle, Journal of Geophysical Research: Atmospheres,
680 114, 10.1029/2008jd009969, 2009.
681 Mbourou, G. N. T., Bertrand, J. J., and Nicholson, S. E.: The Diurnal and Seasonal Cycles of
682 Wind-Borne Dust over Africa North of the Equator, Journal of Applied Meteorology, 36, 868-882,
683 10.1175/1520-0450(1997)036<0868:Tdasco>2.0.Co;2, 1997.
684 McComiskey, A., Ricchiazzi, P., Ogren, J., and Dutton, E.: SGPGET: AN SBDART Module for Aerosol
685 Radiative Transfer, 2021.
686 Mikami, M., Shi, G. Y., Uno, I., Yabuki, S., Iwasaka, Y., Yasui, M., Aoki, T., Tanaka, T. Y., Kurosaki,
687 Y., Masuda, K., Uchiyama, A., Matsuki, A., Sakai, T., Takemi, T., Nakawo, M., Seino, N., Ishizuka, M.,
688 Satake, S., Fujita, K., Hara, Y., Kai, K., Kanayama, S., Hayashi, M., Du, M., Kanai, Y., Yamada, Y.,
689 Zhang, X. Y., Shen, Z., Zhou, H., Abe, O., Nagai, T., Tsutsumi, Y., Chiba, M., and Suzuki, J.: Aeolian
690 dust experiment on climate impact: An overview of Japan–China joint project ADEC, Global and
691 Planetary Change, 52, 142-172, https://doi.org/10.1016/j.gloplacha.2006.03.001, 2006.
692 Miller, R., Knippertz, P., P érez Garc á-Pando, C., Perlwitz, J., and Tegen, I.: Impact of Dust Radiative
693 Forcing upon Climate, in, 327-357, 2014.
694 Mishchenko, M. I., Travis, L. D., and Mackowski, D. W.: T-matrix computations of light scattering by
695 nonspherical particles: A review, Journal of Quantitative Spectroscopy and Radiative Transfer, 55,
696 535-575, https://doi.org/10.1016/0022-4073(96)00002-7, 1996.
697 Mishchenko, M. I., and Travis, L. D.: Capabilities and limitations of a current FORTRAN
698 implementation of the T-matrix method for randomly oriented, rotationally symmetric scatterers, Journal
699 of Quantitative Spectroscopy and Radiative Transfer, 60, 309-324,
700 https://doi.org/10.1016/S0022-4073(98)00008-9, 1998.
701 Mishchenko, M. I., and Travis, L. D.: Gustav Mie and the Evolving Discipline of Electromagnetic
702 Scattering by Particles, Bulletin of the American Meteorological Society, 89, 1853-1862,
703 10.1175/2008bams2632.1, 2008.

Nakajima, T., Tanaka, M., Yamano, M., Shiobara, M., Arao, K., and Nakanishi, Y.: Aerosol Optical Characteristics in the Yellow Sand Events Observed in May, 1982 at Nagasaki-Part II Models, Journal of the Meteorological Society of Japan. Ser. II, 67, 279-291, 10.2151/jmsj1965.67.2_279, 1989.

Okada, K., Heintzenberg, J., Kai, K., and Qin, Y.: Shape of atmospheric mineral particles collected in three Chinese arid-regions, Geophysical Research Letters, 28, 3123-3126, 10.1029/2000gl012798, 2001.

Qie, L., Li, L., Li, K., Li, D., and Xu, H.: Retrieval of aerosol optical properties from ground-based remote sensing measurements: Aerosol asymmetry factor and single scattering albedo, 2019.

Ramanathan, V., Cess, R., Harrison, E., Minnis, P., Barkstrom, B., Ahmad, E., and Hartmann, D.: Cloud-Radiative Forcing and Climate: Results from The Earth Radiation Budget Experiment, Science (New York, N.Y.), 243, 57-63, 10.1126/science.243.4887.57, 1989.

Remer, L. A., Kaufman, Y. J., Tanré, D., Mattoo, S., Chu, D. A., Martins, J. V., Li, R. R., Ichoku, C., Levy, R. C., Kleidman, R. G., Eck, T. F., Vermote, E., and Holben, B. N.: The MODIS Aerosol Algorithm, Products, and Validation, Journal of the Atmospheric Sciences, 62, 947-973, 10.1175/JAS3385.1, 2005.

Ricchiazzi, P., Yang, S., Gautier, C., and Sowle, D.: SBDART: A Research and Teaching Software Tool for Plane-Parallel Radiative Transfer in the Earth's Atmosphere, Bulletin of the American Meteorological Society, 79, 2101-2114, 10.1175/1520-0477(1998)079<2101:Sarats>2.0.Co;2, 1998a.

Ricchiazzi, P., Yang, S., Gautier, C., and Sowle, D.: SBDART: A Research and Teaching Software Tool for Plane-Parallel Radiative Transfer in the Earth's Atmosphere, Bulletin of the American Meteorological Society, 79, 2101, 10.1175/1520-0477(1998)079<2101:Sarats>2.0.Co;2, 1998b.

Román, M. O., Schaaf, C. B., Lewis, P., Gao, F., Anderson, G. P., Privette, J. L., Strahler, A. H., Woodcock, C. E., and Barnsley, M.: Assessing the coupling between surface albedo derived from MODIS and the fraction of diffuse skylight over spatially-characterized landscapes, Remote Sensing of Environment, 114, 738-760, https://doi.org/10.1016/j.rse.2009.11.014, 2010.

Satheesh, S. K., and Ramanathan, V.: Large differences in tropical aerosol forcing at the top of the atmosphere and Earth's surface, Nature, 405, 60-63, 10.1038/35011039, 2000.

Satheesh, S. K.: Letter to the Editor
Aerosol radiative forcing over land: effect of surface and cloud reflection, Ann. Geophys., 20, 2105-2109, 10.5194/angeo-20-2105-2002, 2002.

Satheesh, S. K., and Srinivasan, J.: A Method to Estimate Aerosol Radiative Forcing from Spectral Optical Depths, Journal of Atmospheric Sciences, 63, 1082, 10.1175/jas3663.1, 2006.

734 Sayer, A. M., Munchak, L. A., Hsu, N. C., Levy, R. C., Bettenhausen, C., and Jeong, M.-J.: MODIS
735 Collection 6 aerosol products: Comparison between Aqua's e-Deep Blue, Dark Target, and "merged"
736 data sets, and usage recommendations, Journal of Geophysical Research: Atmospheres, 119,
737 13,965-913,989, 10.1002/2014jd022453, 2014.
738 Schaaf, C., Martonchik, J., Pinty, B., Govaerts, Y., Gao, F., Lattanzio, A., Liu, J., Strahler, A., and
739 Taberner, M.: Retrieval of Surface Albedo from Satellite Sensors, in: Advances in Land Remote Sensing:
740 System, Modeling, Inversion and Application, edited by: Liang, S., Springer Netherlands, Dordrecht,
741 219-243, 2008.
742 Schaaf, C. B., Gao, F., Strahler, A. H., Lucht, W., Li, X., Tsang, T., Strugnell, N. C., Zhang, X., Jin, Y.,
743 Muller, J.-P., Lewis, P., Barnsley, M., Hobson, P., Disney, M., Roberts, G., Dunderdale, M., Doll, C.,
744 d'Entremont, R. P., Hu, B., Liang, S., Privette, J. L., and Roy, D.: First operational BRDF, albedo nadir
745 reflectance products from MODIS, Remote Sensing of Environment, 83, 135-148,
746 https://doi.org/10.1016/S0034-4257(02)00091-3, 2002a.
747 Schaaf, C. B., Gao, F., Strahler, A. H., Lucht, W., Li, X., Tsang, T., Strugnell, N. C., Zhang, X., Jin, Y.,
748 Muller, J.-P., Lewis, P., Barnsley, M., Hobson, P., Disney, M., Roberts, G., Dunderdale, M., Doll, C.,
749 d'Entremont, R. P., Hu, B., Liang, S., Privette, J. L., and Roy, D.: First operational BRDF, albedo nadir
750 reflectance products from MODIS, Remote Sensing of Environment, 83, 135,
751 10.1016/s0034-4257(02)00091-3, 2002b.
752 Schaaf, C. B., Liu, J., Gao, F., and Strahler, A. H.: Aqua and Terra MODIS Albedo and Reflectance
753 Anisotropy Products, in: Land Remote Sensing and Global Environmental Change: NASA's Earth
754 Observing System and the Science of ASTER and MODIS, edited by: Ramachandran, B., Justice, C. O.,
755 and Abrams, M. J., Springer New York, New York, NY, 549-561, 2011.
756 Shi, G., Wang, H., Wang, B., Li, W., Gong, S., Zhao, T., and Aoki, T.: Sensitivity Experiments on the
757 Effects of Optical Properties of Dust Aerosols on Their Radiative Forcing under Clear Sky Condition,
758 Journal of The Meteorological Society of Japan - J METEOROL SOC JPN, 83A, 333-346,
759 10.2151/jmsj.83A.333, 2005.
760 Slingo, A., Ackerman, T. P., Allan, R. P., Kassianov, E. I., McFarlane, S. A., Robinson, G. J., Barnard, J.
761 C., Miller, M. A., Harries, J. E., Russell, J. E., and Dewitte, S.: Observations of the impact of a major
762 Saharan dust storm on the atmospheric radiation balance, Geophysical Research Letters, 33,
763 10.1029/2006gl027869, 2006.

764 Tanré, D., Kaufman, Y., Holben, B., Chatenet, B., Karnieli, A., Lavenu, F., Blarel, L., Dubovik, O.,
765 Remer, L., and Smirnov, A.: Climatology of dust aerosol size distribution and optical properties derived
766 from remotely sensed data in the solar spectrum, Journal of Geophysical Research, 106,
767 10.1029/2000JD900663, 2001.
768 Tegen, I., Bierwirth, E., Heinold, B., Helmert, J., and Wendisch, M.: Effect of measured surface albedo
769 on modeled Saharan dust solar radiative forcing, Journal of Geophysical Research: Atmospheres, 115,
770 10.1029/2009jd013764, 2010.
771 Textor, C., Schulz, M., Guibert, S., Kinne, S., Balkanski, Y., Bauer, S., Berntsen, T., Berglen, T.,
772 Boucher, O., Chin, M., Dentener, F., Diehl, T., Feichter, J., Fillmore, D., Ginoux, P., Gong, S., Grini, A.,
773 Hendricks, J., Horowitz, L., Huang, P., Isaksen, I. S. A., Iversen, T., Kloster, S., Koch, D., Kirkevåg, A.,
774 Kristjansson, J. E., Krol, M., Lauer, A., Lamarque, J. F., Liu, X., Montanaro, V., Myhre, G., Penner, J. E.,
775 Pitari, G., Reddy, M. S., Seland, Ø., Stier, P., Takemura, T., and Tie, X.: The effect of harmonized
776 emissions on aerosol properties in global models – an AeroCom experiment, Atmos. Chem. Phys., 7,
777 4489-4501, 10.5194/acp-7-4489-2007, 2007.
778 Tian, L., Zhang, P., and Chen, L.: Estimation of the Dust Aerosol Shortwave Direct Forcing Over Land
779 Based on an Equi-albedo Method From Satellite Measurements, Journal of Geophysical Research:
780 Atmospheres, 124, 8793-8807, 10.1029/2019JD030974, 2019.
781 Valenzuela, A., Olmo, F. J., Lyamani, H., Antón, M., Quirantes, A., and Alados-Arboledas, L.: Aerosol
782 radiative forcing during African desert dust events (2005–2010) over Southeastern Spain, Atmospheric
783 Chemistry and Physics (ACP) & Discussions (ACPD), 2012.
784 Wang, Z., Zhang, H., Jing, X., and Wei, X.: Effect of non-spherical dust aerosol on its direct radiative
785 forcing, Atmospheric Research, 120-121, 112-126, https://doi.org/10.1016/j.atmosres.2012.08.006,
786 2013.
787 Wielicki, B. A., Barkstrom, B. R., Baum, B. A., Charlock, T. P., Green, R. N., Kratz, D. P., Lee, R. B.,
788 Minnis, P., Smith, G. L., Takmeng, W., Young, D. F., Cess, R. D., Coakley, J. A., Crommelynck, D. A.
789 H., Donner, L., Kandel, R., King, M. D., Miller, A. J., Ramanathan, V., Randall, D. A., Stowe, L. L., and
790 Welch, R. M.: Clouds and the Earth's Radiant Energy System (CERES): algorithm overview, IEEE
791 Transactions on Geoscience and Remote Sensing, 36, 1127-1141, 1998.
792 Xia, X., and Zong, X.: Shortwave versus longwave direct radiative forcing by Taklimakan dust aerosols,
793 Geophysical Research Letters, 36, 10.1029/2009gl037237, 2009.

794 Zhang, J., Christopher, S. A., Remer, L. A., and Kaufman, Y. J.: Shortwave aerosol radiative forcing
795 over cloud-free oceans from Terra: 2. Seasonal and global distributions, Journal of Geophysical
796 Research (Atmospheres), 110, D10S24, 2005.
797 Zhang, P., Lu, N.-m., Hu, X.-q., and Dong, C.-h.: Identification and physical retrieval of dust storm using
798 three MODIS thermal IR channels, Global and Planetary Change, 52, 197-206,
799 https://doi.org/10.1016/j.gloplacha.2006.02.014, 2006.
800 Zhao, C., Chen, S., Leung, L. R., Qian, Y., Kok, J. F., Zaveri, R. A., and Huang, J.: Uncertainty in
801 modeling dust mass balance and radiative forcing from size parameterization, Atmos. Chem. Phys., 13,
802 10733-10753, 10.5194/acp-13-10733-2013, 2013.
803